Bioorganic Chemistry 82 (2019) 211–223

Contents lists available at ScienceDirect

Bioorganic Chemistry

journal homepage: www.elsevier.com/locate/bioorg

Design and development of novel p-aminobenzoic acid derivatives as potential cholinesterase inhibitors for the treatment of Alzheimer's disease

Sushant K. Shrivastava[a,*], Saurabh K. Sinha[b], Pavan Srivastava[a], Prabhash N. Tripathi[a], Piyoosh Sharma[a], Manish K. Tripathi[a], Avanish Tripathi[a], Priyanka K. Choubey[a], Digambar K. Waiker[a], Lalit M. Aggarwal[c], Manish Dixit[d], Subhash C. Kheruka[d], Sanjay Gambhir[d], Sharmila Shankar[e], Rakesh K. Srivastava[f]

[a] Pharmaceutical Chemistry Research Laboratory, Department of Pharmaceutical Engineering & Technology, Indian Institute of Technology (Banaras Hindu University), Varanasi 221005, U.P., India
[b] Department of Pharmaceutical Sciences, Mohanlal Sukhadia University, Udaipur 313001, Rajasthan, India
[c] Department of Radiotherapy & Radiation Medicine, Institute of Medical Sciences, Banaras Hindu University, Varanasi, UP 221 005, India
[d] Department of Nuclear Medicine, SGPGIMS, Raebareli Road, Lucknow 226014, UP, India
[e] Department of Genetics, Louisiana State University Health Sciences Center, 1700 Tulane Avenue, New Orleans, LA 70112, USA
[f] Stanley S. Scott Cancer Center, Louisiana State University Health Sciences Center, 1700 Tulane Avenue, New Orleans, LA 70112, USA

ARTICLE INFO

Keywords:
Anticholinesterase
p-Aminobenzoic acid
Working and reference memory
Molecular dynamics
Antiamnesic

ABSTRACT

Based on the quantitative structure-activity relationship (QSAR), some novel p-aminobenzoic acid derivatives as promising cholinesterase enzyme inhibitors were designed, synthesized, characterized and evaluated to enhance learning and memory. The *in vitro* enzyme kinetic study of the synthesized compounds revealed the type of inhibition on the respective acetylcholinesterase (AChE) and butyrylcholinesterase (BChE) enzymes. The *in vivo* studies of the synthesized compounds exhibited significant reversal of cognitive deficits in the animal models of amnesia as compared to standard drug donepezil. Further, the *ex vivo* studies in the specific brain regions like the hippocampus, hypothalamus, and prefrontal cortex regions also exhibited AChE inhibition comparable to standard donepezil. The *in silico* molecular docking and dynamics simulations studies of the most potent compound **22** revealed the consensual interactions at the active site pocket of the AChE.

1. Introduction

The Alzheimer's Disease (AD) generally occurs due to the progressive dysfunctioning of cholinergic neurons and also due to the β-amyloid accumulation in some selected portions of the brain, namely hippocampus, and the cortex, which resulted into a decline of learning and memory [1–3]. AD in its early stage begins with the early symptoms of cognitive dysfunctioning, which gradually leads to complete loss of memory and ultimately become fatal. According to World Health Organization (WHO) report on the AD, around 36 million population worldwide were living with dementia till 2010; this figure would be increased up to 66 million by 2030 and 115 million by 2050 [4]. It was also revealed that death due to AD had been increased by 68% over the past decade, whereas the death rate in case of many other diseases had been decreased over the years, such as heart disease (16%), stroke (23%), and prostate cancer (8%) [5,6]. Therefore, the discovery of new molecules for the treatment of AD remains a big challenge for the healthcare community. Several molecular mechanisms and hypothesis have been proposed till date, which suggested the potential role of acetylcholine (ACh), amyloid beta (Aβ) protein, NMDA receptor, tau neurofibrillary tangles, oxidative stress biomarkers, etc. [7–9]. The role of ACh deficiency is well known to be associated with the AD, and for the last five decades, acetylcholinesterase inhibitors (AChEIs) are the most prescribing drugs for the treatment of AD. Currently, there are only four drugs approved for the treatment of AD and amongst these, three are AChEIs (donepezil, rivastigmine, and galantamine). The clinical outcomes of these approved drugs include symptomatic relief from cognitive dysfunctionalities without modifying the disease functions. Therefore, the ultimate goal of the researchers is to find and develop a preventive as well as curative treatment of AD.

The AD is associated with aging, and geriatric individuals are more prone to developing the disease [10]. Since rats and humans exhibit comparable age-related behavioral alterations [11,12], and the aged rats also provide useful insight into human age-related deficits by

* Corresponding author.
E-mail address: skshrivastava.phe@iitbhu.ac.in (S.K. Shrivastava).

https://doi.org/10.1016/j.bioorg.2018.10.009
Received 16 July 2018; Received in revised form 2 October 2018; Accepted 4 October 2018
Available online 09 October 2018
0045-2068/

examining their related cognitive impairment and spatial memory deficits [13]. The working and reference memory are widely acknowledged to study learning and memory [14]. The reference memory is long-term memory acquired by repetitive training and is exemplified by learning the rules to perform any task (like swimming to a platform). On the other side, working memory can be described as a type of short-term memory in which useful information is retained [15]. In some of our previous studies, we have developed 4-aminopyridine derivatives (Schiff bases imide, anilide, and semicarbazones) with potential AChE inhibitory potential to improve learning and memory [16–18]. Also, there were several derivatives of *m*- and *p*-aminobenzoic acid (amide and imide derivatives) synthesized and evaluated as cholinesterase inhibitors, which suggested that *p*-substituted derivatives were more active than *m*- and *o*-substituted derivatives [19,20]. These observations were taken into account to design a novel series of p-aminobenzoic acid derivatives linked with semicarbazones.

In this study, we have selected various p-aminobenzoic acid and semicarbazone derivatives reported in our previous reports with diverse AChE inhibitory activity to generate a field-based 3D-QSAR model and identified the several physicochemical features of the reported molecules through contour maps. The physicochemical features of the best compound were further utilized to design and screen the novel p-aminobenzoic acid derivatives. The identified screened compounds were further synthesized, characterized, and pharmacologically evaluated for memory-enhancing properties associated with anticholinesterase activities in aged rats.

2. Results and discussion

2.1. Field-based Gaussian 3D QSAR analysis

The QSAR model enriched with electrostatic, hydrophobic, and steric fields was generated by field-based Gaussian QSAR model that helped to understand the relationship between the chemical functionalities of a set of aligned ligands and their known biological activity in a three-dimensional grid to optimize the lead compounds. The partial least-squares (PLS) analysis was used to establish a relationship between the biological activity and respective fields, i.e., electrostatic, steric, hydrophobic, hydrogen bond donor (HBD), and hydrogen bond acceptor HBA). The actual pIC_{50} values of the reported ligands from our previous work were used for calculation of experimental pIC_{50} values (See Supplementary Table S1). The leave-one-out method of cross-validation was used to access the predictive abilities of the model. The accuracy or usefulness of the model was statistically significant according to leave-one-out cross-validation with $R^2 > 0.6$, $R^2CV > 0.5$, larger F value, smaller P-value, and external set predictive capacity (R^2 test > 0.5) [21]. Out of the generated model, the third model showed the statistically significant R^2 value of 0.7972 for the training set, Q^2 of 0.7135, cross-validated correlation coefficient (R^2CV) of 0.5429, the sum of squared deviation (SD) of 0.2786, F value 33.6 and Pearson-R of 0.8491 (See Supplementary Tables S2 and S3). The obtained statistical parameter showed good internal predictivity of the developed model. The statistical parameter and the field fractions were calculated for the predicted model. The model provided the field fraction values, which showed the contribution of five feature field-intensities such as steric, electrostatic, hydrophobic, HBD, and HBA were found 0.38, 0.09, 0.17, 0.24, and 0.12 respectively. The correlation between the experimental and training test data sets showed a significant correlation between the predicted and experimental values with the R^2 value of the test set to be 0.8655 (Fig. 1). The field intensities of steric, hydrophobic and HBA indicated that these features are essential for the protein-ligand interactions. Further, the contour maps were generated by Gaussian-based 3D QSAR model around the most active compound C9 as shown in Fig. 2.

The blue region around the phenyl ring A and B (See Supplementary Fig.S4) showed favorable steric region (Fig. 2). Thus, we added the carboxylic, hydroxyl, and methoxy group in the phenyl ring of the designed series to increase the steric bulk. In the hydrophobic contour maps, the presence of both negative and positive contours indicated that the substitution around the para position of the phenyl ring B & C was of utmost importance. Thus, to check the influence of hydrophobicity in the designed compounds, we substituted both the hydrophilic groups (like hydroxyl) and hydrophobic groups (like phenyl and methoxy) around the phenyl ring B and C. Similarly, the hydrogen bond and electrostatic contour maps also guided the designing of new compounds. Further, based on the QSAR study and contour maps analysis, the activity of the designed compounds against AChE was predicted (pIC_{50}) (See Supplementary Table S4).

2.2. Chemistry

The target compounds were synthesized in accordance with Scheme 1. p-aminobenzoic acid **(1)** was reacted in alkaline condition with ethyl chloroformate in the presence of 1,4-dioxane:water (1:1) to yield 4-(ethoxycarbonylamino) benzoic acid **(2)**.

FT-IR, ^{1}H NMR, and ^{13}C NMR techniques were used for the characterization of the synthesized compounds. The FT-IR peaks observed at 1630–1590 cm^{-1} and 3433–3326 cm^{-1} showed the presence of C═N and −NH groups respectively. A series of 20 compounds (**4–23**) were synthesized based on nucleophilic attack of (**3**) on corresponding aromatic aldehydes or aromatic ketones. The ^{1}H NMR spectra of compounds (**4–11**) showed a resonance between δ 8.34–6.65 ppm, which established the presence of the aromatic and −N═CH protons. In compounds (**12–23**), the −N═CH proton was substituted by different groups (methyl, ethyl, and substituted or unsubstituted phenyl), confirming the formation of N═C bond based on the disappearance of the −N═CH proton peak. The ^{13}C NMR resonances around δ 145 and 162 ppm confirmed the N═CH and N═C bond formation, respectively.

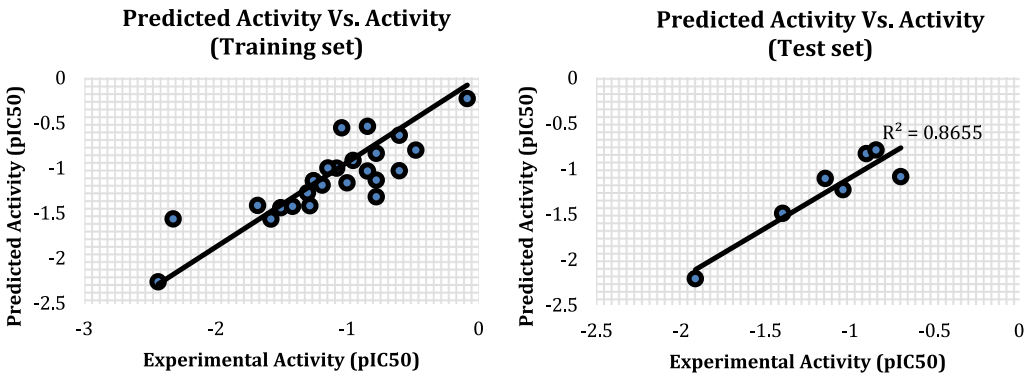

Fig. 1. The scattered plot between experimental and predicted activity values using field-based 3D-QSAR model. (a) Training set compounds and (b) Test set compounds.

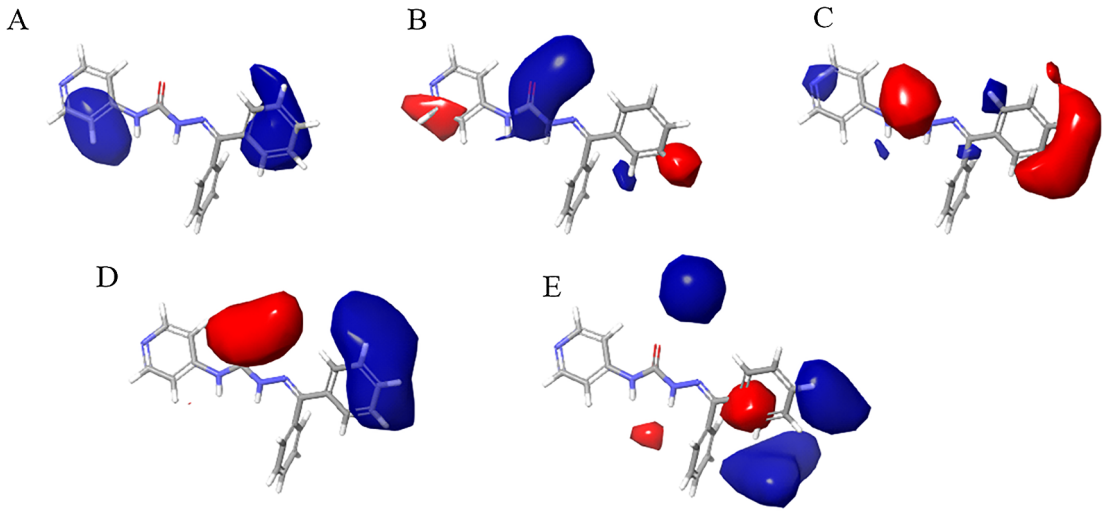

Fig. 2. QSAR contour map representation of the most active ligand S9 with both positive (blue) and negative (red) field distribution of the respective feature (A) Steric (B) Electrostatic (C) Hydrophobic (D) HBA (E) HBD. Blue regions indicated favorable changes and red regions represented as unfavorable features of compounds.

To measure the purity of the synthesized compounds, elemental analyses and thin layer chromatography (TLC) studies were carried out. The "shake-flask" method (*n*-octanol/water) was used to determine the Log P (partition coefficient) values of the synthesized compounds. The Rf values, melting point and Log P values of the title compounds are given in Table 1.

2.3. Cholinesterase inhibition

The cholinesterase activity of the synthesized compounds was evaluated using the Ellman's method. AChE was obtained from the electric eel (E.C. 3.1.1.7) and butyrylcholinesterase from human serum (E.C. 3.1.1.8). According to the IC_{50} data (Table 2), replacement of the hydrogen of imine carbon (−N═CH) of semicarbazone in compounds **(12–23)** displayed an increase in activity. The selectivity towards AChE was increased with the presence of lipophilic ring substituents (phenyl) in compounds **(18–23)** and decreased with the presence of shorter alkyl ($-CH_3/-C_2H_5$) chain in compounds **(12–17)**. Compounds **(18, 21 and 22)**, in which the hydrogen atom was substituted by an aromatic (phenyl) moiety, exhibited significant AChE inhibition (0.056 ± 0.02,

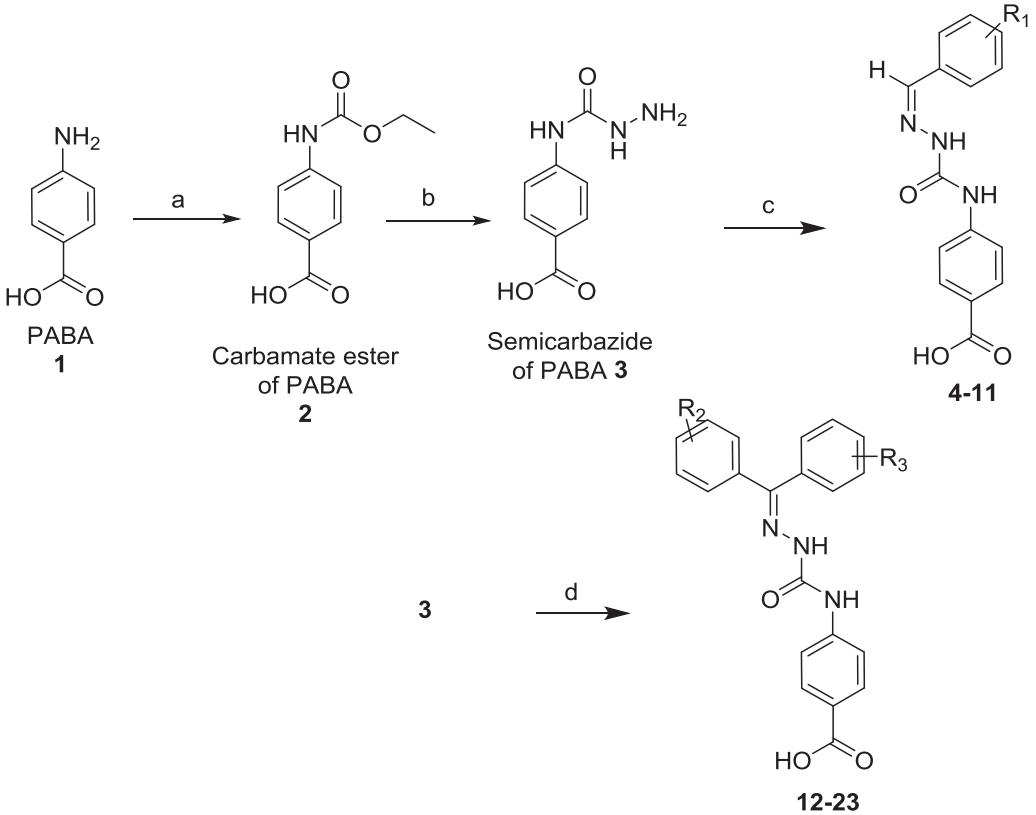

Scheme 1. Synthesis of target compounds **4–23**. Reagents and conditions: (a) ethyl chloroformate, Dioxane: Water (1:1), 1 M NaOH, overnight; (b) hydrazine hydrate, absolute ethanol, reflux, 2–3 h; (c) substituted aldehyde, absolute ethanol, reflux, 4–6 h; (d) substitutes benzophenone, benzene, Molecular Sieve 4A, 20 min.

Table 1
Chemical structures and physicochemical properties of the synthesized compounds.

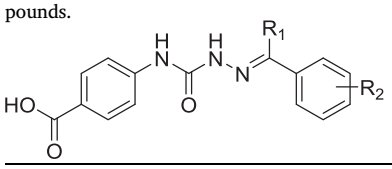

Comp.	R_1	R_2	Rf[a]	Melting point (°C)[b]	Log P[c]
4	H	H	0.64	210–212	2.86
5	H	2-OH	0.51	245–247	1.48
6	H	2,4-diOH	0.63	256–258	0.98
7	H	2,4,6-triOH	0.56	242–244	0.52
8	H	2-OCH_3	0.54	172–174	2.98
9	H	2,4-diOCH_3	0.48	165–167	3.36
10	H	2,4,6-triOCH_3	0.65	158–160	3.86
11	H	4-OH-3,5-diOCH_3	0.47	178–180	2.44
12	CH_3	H	0.58	240–242	3.30
13	CH_3	4-OCH_3	0.62	236–238	3.68
14	CH_3	4-OH-3-OCH_3	0.55	195–197	3.18
15	C_2H_5	H	0.46	184–186	3.61
16	C_2H_5	4-OCH_3	0.45	132–134	3.94
17	C_2H_5	4-OH-3-OCH_3	0.66	148–150	3.18
18	C_6H_5	H	0.56	222–224	3.87
19	C_6H_5	4-OCH_3	0.48	214–216	4.29
20	4-$OCH_3C_6H_5$	4-OCH_3	0.41	242–244	4.48
21	C_6H_5	4-OH	0.42	177–179	3.67
22	4-OHC_6H_5	4-OH	0.68	156–158	3.13
23	4-OHC_6H_5	4,6-diOCH_3	0.47	223–225	3.84

[a] Rf determined using a mixture of ethyl acetate: pyridine: acetic acid: water (100:18.5:2.5:5) as the solvent system.
[b] Melting points (non-corrected) calculated on BI 9300 Bumstead/Electrothermal Stuart (SMPIO) melting point apparatus in open capillary tubes.
[c] Log P values calculated by the shake flask method.

0.05 ± 0.01 and 0.046 ± 0.01 μM, respectively) comparable to donepezil (0.04 ± 0.01 μM). Compounds **(12–17)**, in which the hydrogen was substituted by methyl or ethyl moieties, exhibited increased AChE and BChE inhibitory activity. The methyl-substituted compounds **(12–14)** exhibited better BChE inhibitory activity than the ethyl-substituted compounds **(15–17)**. The compound **(12)** demonstrated good inhibitory activity against both the enzymes.

Further, the synthesized derivatives were subjected to enzyme kinetics studies [22], and results are reported in Table 3. The most active compound **(22)** exhibited non-competitive inhibition of AChE and BChE (Ki = 0.041 ± 0.60 μM and 8.46 ± 0.66 μM). This non-competitive inhibition might be due to the interaction between the compound **(22)**, and the peripheral anionic site (PAS) of AChE showed by the molecular docking and dynamics simulation studies.

2.4. Biological evaluations

The top four compounds on the basis of their significant AChE inhibition potential were further selected to assess their role in improving the reference and working memory using the Morris water maze test. The spatial reference memory data was observed by using two-way ANOVA revealed significant differences in escape latency amongst compound-treated groups {$F(2, 165) = 4383$, $p < 0.05$} and times {$F(10, 165) = 481.6$, $p < 0.05$}. Further, there exist a significant difference between the compound-treated groups and time {$F(20, 165) = 7.93$, $p < 0.05$}. Additionally, significant differences were found in the swim distance amongst compound-treated groups {$F(2, 165) = 918434$, $p < 0.05$} and times {$F(10, 165) = 345153$, $p < 0.05$}. A significant interaction was found between compound-treated groups and time {$F(20, 165) = 4537$, $p < 0.05$} (Table 4). Post-hoc analysis showed that compounds **(12, 18, 21, and 22)** and donepezil significantly decreased the escape latency and swim distance to reach a hidden platform on days 7, 8 and 9 compared to the control. The probe trial was conducted after twenty-four hours of spatial reference memory task, to evaluate whether this memory trace retained and consolidated for the future navigation. In the probe trial one way ANOVA reveals significant differences {$F(10, 55) = 132.9$, $p < 0.05$} amongst the groups. Post hoc analysis indicated that mean time spent by rats treated with compounds **(12, 18, 21,** and **22)** and donepezil in the target quadrant of the maze was found to be significantly longer than the control group. The time spent by rats in the target quadrant during the probe trial showed the retention of spatial memory. For testing the spatial working memory, it was expected that rat finds a platform placed in a new position through the first trial (acquisition), whereas in retrieval trial, the platform was kept to its previous position.

Table 2
IC_{50} values of synthesized compounds.

Comp.	R_1	R_2	AChE IC_{50} (μM) ± SEM	BChE IC_{50} (μM) ± SEM	Selectivity for AChE[a]
4	H	H	42.50 ± 3.98	> 1000	–
5	H	2-OH	10.20 ± 1.75	882.6 ± 1.76	86.53
6	H	2,4-diOH	2.14 ± 0.60	171.2 ± 1.60	80.01
7	H	2,4,6-triOH	20.60 ± 1.20	955.8 ± 1.92	46.40
8	H	2-OCH_3	64.80 ± 1.60	> 1000	–
9	H	2,4-diOCH_3	89.30 ± 1.20	> 1000	–
10	H	2,4,6-triOCH_3	114.5 ± 1.75	> 1000	–
11	H	4-OH-3,5-diOCH_3	108.4 ± 1.40	> 1000	–
12	CH_3	H	0.126 ± 0.60	1.11 ± 0.76	8.83
13	CH_3	4-OCH_3	8.34 ± 0.60	7.71 ± 1.20	0.92
14	CH_3	4-OH-3-OCH_3	7.52 ± 0.57	5.84 ± 1.75	0.78
15	C_2H_5	H	4.71 ± 0.76	10.01 ± 0.65	2.13
16	C_2H_5	4-OCH_3	28.6 ± 0.65	12.49 ± 2.81	0.44
17	C_2H_5	4-OH-3-OCH_3	21.7 ± 0.60	11.54 ± 1.76	0.53
18	C_6H_5	H	0.056 ± 0.02	22.19 ± 0.42	396.25
19	C_6H_5	4-OCH_3	6.45 ± 0.76	709.5 ± 3.98	110.00
20	4-$OCH_3C_6H_5$	4-OCH_3	15.82 ± 0.42	> 1000	–
21	C_6H_5	4-OH	0.050 ± 0.01	15.14 ± 0.65	302.80
22	4-OHC_6H_5	4-OH	0.046 ± 0.01	16.96 ± 0.76	368.70
23	4-OHC_6H_5	4,6-diOCH_3	8.36 ± 0.57	> 1000	–
Don	–	–	0.040 ± 0.01	15.24 ± 0.42	381.00
Riva*	–	–	2.25 ± 0.66	1.66 ± 0.44	0.74

[a] Selectivity for AChE is defined as IC_{50} (BChE)/IC_{50} (AChE).
* Data taken from (Sheng et al., 2009) [23]; Don = Donepezil; Riva = Rivastigmine.

Table 3
Enzyme kinetics study of the synthesized compounds.

Comp.	Types of inhibition (AChE)	AChE Ki (μM) ± SEM	Types of inhibition (BChE)	BChE Ki (μM) ± SEM
4	nt	38.27 ± 1.48	nt	nt
5	nt	9.14 ± 0.94	nc	850.36 ± 4.47
6	c	1.54 ± 0.66	c	164.58 ± 2.64
7	c	17.35 ± 0.80	nc	941.2 ± 4.47
8	c	55.23	nt	nt
9	c	80.69 ± 1.48	nt	nt
10	c	110.25 ± 1.26	nt	nt
11	c	104.65 ± 0.60	nt	nt
12	nc	0.11 ± 0.66	c	1.05 ± 0.73
13	nc	7.84 ± 0.42	c	7.21 ± 0.58
14	nc	6.12 ± 0.86	nc	5.25 ± 0.80
15	nc	2.89 ± 0.84	nc	9.28 ± 0.90
16	nc	25.84 ± 0.80	c	11.85 ± 1.27
17	nc	20.35 ± 0.94	nc	11.26 ± 1.48
18	nc	0.044 ± 0.65	c	20.24 ± 0.76
19	nc	5.36 ± 0.76	nc	642.4 ± 4.47
20	nc	13.85 ± 0.42	nt	nt
21	nc	0.048 ± 0.60	c	14.66 ± 0.84
22	nc	0.041 ± 0.60	nc	15.85 ± 0.66
23	nc	7.52 ± 0.90	nt	nt
Don	nc	0.036 ± 0.02	nc	14.54 ± 0.76

c = competitive; nc = non-competitive; nt = not tested; Don = Donepezil.

Compounds **(18, 21,** and **22)** improved the working memory at doses of 5 and 10 mg/kg; however, compound **(12)** administered at 5 mg/kg was not found to be significantly different from the control. The two-way ANOVA revealed significant differences in the escape latency amongst the compound-treated groups {F (3, 220) = 3920, $p < 0.05$} and times {F (10, 220) = 442.7, $p < 0.05$} (Table 5). Further, significant interactions between the compound-treated groups and time {F (30, 220) = 11.63, $p < 0.05$} were observed. Similarly, analysis of the retrieval trial data showed significant differences amongst groups {F (3, 220) = 3009, $p < 0.05$} and times {F (10, 220) = 560.2, $p < 0.05$}. Significant interactions were also observed between compound-treated groups and time {F (30, 220) = 11.20, $p < 0.05$} (Table 5).

A substantial ($p < 0.05$) difference in the escape latency between the treatment and control groups was observed, which confirmed the improvement in working memory within the trial. A significant difference between days confirmed the daily improvement in working memory because the rats had to solve a new task each day. The working memory is short-term memory system which found to be involved in temporary storage, manipulation of information and simultaneous processing, which are necessary to perform complex cognitive functions efficaciously [23,24]. The information retrieval from long-term memory is also an important component in the memory working [25,26]. Any new information that receives attention enters the working memory system, where it is passively and temporarily stored. This initial short-term information might be transferred into the long-term episodic representations, which can be recalled minutes or even year later [27,28]. Compounds **(12, 18, 21, and 22)** were tested in a scopolamine-induced amnesic model to examine their effectiveness in the reversing learning and memory deficits. This effectiveness is evaluated using the passive avoidance test. In this test, during the training session animal receives a punishment while entering a dark room and it has to remember the session on the following day unless the memory is impaired due to the amnesic drug. The effects of compounds **(12, 18, 21, and 22)** on changes in entry latency in animals with scopolamine-induced amnesia showed significant differences {$p < 0.05$} amongst the treated groups (Table 6). Post-hoc analysis showed that scopolamine (1.5 mg/kg) significantly {$p < 0.05$} decreased entry latency as compared to the control group, which indicated amnesia. Compounds **(12, 18, 21, and 22)** and donepezil dose-dependently reversed scopolamine-induced amnesia.

Further, the study was extended to observe the effects of compounds **(12, 18, 21, and 22)** and donepezil in different regions of the brain. The hippocampus, hypothalamus, and prefrontal cortex were examined due to their involvement in the memory processing through the innervations of cholinergic neurons, and loss of these neurons occurs in demented AD patients [29]. The hippocampus is involved in the temporary storage of information that needs to be acquired and retrieved. This stored information is then transmitted to the prefrontal cortex where conversion of short-term memory into the long-term memory occurs via the process called consolidation [30,31]. Numerous preclinical studies report that hypothalamus stimulation accelerates hippocampus-dependent learning and memory progressions in the rats [32]. Therefore, *ex vivo* AChE activity was revealed that compounds **(12, 18, 21, and 22)** and donepezil displays AChE inhibition activity in the separate brain regions as compared to the control {$p < 0.05$} (Table 7). Thus obtained results confirmed the ability of these compounds to enhance the cholinergic neurotransmission in these separate brain regions and to enhance learning and memory functions due to their anticholinesterase activity. The rats exhibited not any symptom of toxicity and mortality up to a dose of 100 mg/kg of body weight, as

Table 4
Effect of synthesized derivatives and donepezil on spatial reference memory (SRM), and retention of memory in the Morris water maze experiment.

Treatment {Dose (mg/kg)}	Spatial reference memory						Retention of memory
	Day 7		Day 8		Day 9		Time spent in the target quadrant (probe trial on Day 10)
	Escape latency (s)	Swim Distance (cm)	Escape latency (s)	Swim Distance (cm)	Escape latency (s)	Swim Distance (cm)	
Control	56.83 ± 0.60	1100 ± 0.57	40.50 ± 0.76	1000 ± 0.60	28.50 ± 0.76[a]	900.5 ± 0.76[a]	15.50 ± 0.76
12 (5.0)	50.50 ± 0.76	900.2 ± 0.49	31.83 ± 0.60	600.1 ± 0.76	26.33 ± 0.80[b]	400.2 ± 0.57[b]	20.17 ± 0.60*
12 (10.0)	48.50 ± 0.76	800.6 ± 0.79	29.33 ± 0.49	550.5 ± 0.57	21.00 ± 0.57[b]	350.1 ± 0.66[b]	22.67 ± 0.66*
18 (5.0)	40.17 ± 0.60	700.1 ± 0.60	25.17 ± 0.60	400.2 ± 0.47	19.33 ± 0.49[b]	275.5 ± 0.47[b]	28.17 ± 0.60*
18 (10.0)	37.50 ± 0.42	600.5 ± 0.76	21.50 ± 0.42	350.8 ± 0.80	18.00 ± 0.57[b]	225.5 ± 0.60[b]	31.17 ± 0.60*
21 (5.0)	38.17 ± 0.60	550.8 ± 0.49	24.33 ± 0.66	300.2 ± 0.49	18.83 ± 0.47[b]	200.6 ± 0.79[b]	28.00 ± 0.57*
21 (10.0)	36.33 ± 0.49	500.2 ± 0.47	21.17 ± 0.60	250.2 ± 0.76	15.00 ± 0.57[b]	150.2 ± 0.80[b]	30.83 ± 0.47*
22 (5.0)	35.83 ± 0.47	525.4 ± 0.57	20.00 ± 0.57	275.5 ± 0.79	12.50 ± 0.42[b]	200.2 ± 0.49[b]	35.17 ± 0.60*
22 (10.0)	32.17 ± 0.60	490.7 ± 0.60	15.83 ± 0.60	225.6 ± 0.66	7.83 ± 0.47[b]	150.1 ± 0.47[b]	38.67 ± 0.80*
Donepezil (5.0)	33.83 ± 0.60	510.9 ± 0.80	20.00 ± 0.57	270.5 ± 0.60	12.67 ± 0.55[b]	190.8 ± 0.79[b]	35.50 ± 0.76*
Donepezil (10.0)	30.17 ± 0.60	480.3 ± 0.66	15.00 ± 0.57	220.1 ± 0.49	6.83 ± 0.60[b]	145.6 ± 0.49[b]	38.33 ± 0.66*

Values are expressed as mean ± SEM (n = 6).
[a] $p < 0.05$ compared to day 7 of control.
[b] $p < 0.05$ compared to day 9 of control (two way ANOVA followed by Bonferroni post-tests); For probe trial data were analyzed by one way ANOVA.
* $p < 0.05$ compared control.

Table 5
Effect of synthesized derivatives and donepezil on spatial working memory in the Morris water maze experiment.

Treatment {Dose(mg/kg)}	Spatial working memory							
	Acquisition trial Escape latency of first trial (s)				Retrieval trial Escape latency of second trial (s)			
	Day 13	Day 14	Day 15	Day 16	Day 13	Day 14	Day 15	Day 16
Control	54.33 ± 0.66	39.67 ± 0.66	25.50 ± 0.76	24.83 ± 0.70[a]	54.83 ± 0.70	37.50 ± 0.61	27.00 ± 0.63	25.83 ± 0.60[a]
12 (5.0)	51.83 ± 0.60*	36.00 ± 0.63*	23.83 ± 0.60*	24.50 ± 0.61[n]	51.83 ± 0.60	35.00 ± 0.63	25.33 ± 0.49*	24.17 ± 0.60[n]
12 (10.0)	50.83 ± 0.60*	32.83 ± 0.60*	22.67 ± 0.66*	22.83 ± 0.60[b]	50.67 ± 0.49	33.17 ± 0.87	23.67 ± 0.66*	23.50 ± 0.76[b]
18 (5.0)	37.83 ± 0.70*	20.33 ± 0.49*	17.17 ± 0.60*	17.33 ± 0.80[b]	38.00 ± 0.63	20.17 ± 0.60	17.17 ± 0.60*	17.33 ± 0.49[b]
18 (10.0)	35.83 ± 0.60*	25.17 ± 0.60*	16.17 ± 0.79*	16.17 ± 0.87[b]	35.50 ± 0.61	25.17 ± 0.60	15.83 ± 0.60*	16.67 ± 0.49[b]
21 (5.0)	34.17 ± 0.60*	21.83 ± 0.60*	14.83 ± 0.60*	15.50 ± 0.76[b]	32.83 ± 0.60	22.17 ± 0.60	13.33 ± 0.80*	13.83 ± 0.60[b]
21 (10.0)	30.00 ± 0.57*	19.17 ± 0.60*	10.67 ± 0.49*	10.33 ± 0.66[b]	31.17 ± 0.60	18.83 ± 0.60	11.17 ± 0.60*	10.33 ± 0.49[b]
22 (5.0)	33.83 ± 0.70*	22.00 ± 0.63*	15.17 ± 0.60*	14.83 ± 0.60[b]	31.83 ± 0.60	21.17 ± 0.79	13.17 ± 0.60*	13.67 ± 0.66[b]
22 (10.0)	30.17 ± 0.60*	19.33 ± 0.80*	10.17 ± 0.60*	9.83 ± 0.60[b]	30.17 ± 0.60	16.67 ± 0.66	10.17 ± 0.60*	11.00 ± 0.63[b]
Donepezil (5.0)	35.17 ± 0.60*	21.00 ± 0.57*	14.50 ± 0.76*	14.00 ± 0.63[b]	30.00 ± 0.57	19.67 ± 0.66	13.00 ± 0.63*	11.83 ± 0.60[b]
Donepezil (10.0)	31.00 ± 0.63*	20.33 ± 0.71	10.33 ± 0.49*	9.83 ± 0.60[b]	30.17 ± 0.60	15.33 ± 0.80	9.33 ± 0.42*	9.00 ± 0.36[b]

Values are expressed as mean ± SEM (n = 6); Data were analyzed by two way ANOVA followed by Bonferroni post-tests.
[a] $p < 0.05$ compared to day 13 of control.
[b] $p < 0.05$ compared to day 16 of control.
* $p < 0.05$ compared to control; n = non-significant to control.

evident during the period of observation in the normal behavioral pattern in the rats. In the open field test, it was observed that synthesized compounds found not to reduce the locomotor activity in the rats. Rats treated with the most active compound **(22)** exhibited 42 ± 8 line crossings and a rearing frequency of 3.6 ± 1.8 in 3 min, which is comparable with the control (43 ± 6 crossings and 4 ± 1.2 rearings in 3 min) (See Supplementary Tables S5 and S6).

2.5. Molecular docking studies

Glide module of the Schrödinger Maestro was used to perform molecular docking studies of the most potent compound **(22)** on AChE protein structure (PDB Code: 1EVE) [33]. The docking simulations provide insights into the possible binding mode and binding interactions between protein and ligand. Firstly, the parameters of docking experiment and prepared gird structure were validated by performing re-docking of the co-crystallized structure of donepezil and using the superposition tool to calculate RMSD value, which was found to be within the acceptable limit of 2 Å (Fig. 3A) [34]. Also, the binding pose and active site interactions of donepezil on AChE was also validated (Fig. 3B), which confirmed the suitability of docking protocols and prepared grid.

Further, the docking simulations of compound **(22)** revealed that ligand was found to interact with both the catalytic and peripheral site of AChE. The detailed analysis of the docked complex suggested that compound **(22)** is oriented by lining along with the His440 residue of the catalytic site and interacted through polar interaction. The biphenyl portion with a *p*-hydroxy substituent in compound **(22)** occupied the PAS and interacted with Trp279 through π-π stacking interaction. The compound **(22)** was also found to be involved in interactions with other PAS residues such as Tyr70, Try121, and Tyr334 by hydrophobic and Asp72 through charged interaction. Apart from the interactions with residues of CAS and PAS, the compound **(22)** also interacted with acyl binding pocket (Phe288, Phe290, and Phe331), anionic subsite (Phe330), and other amino acid residues (Leu282, Phe284, Ser286, Ile287, Arg289, Phe331, and Tyr334) (Fig. 4A and B). All these interactions were observed within the radius of 4 Å.

The detailed and comparative docking analysis of compound **(22)** and donepezil revealed that compound **(22)** occupied the similar docking pose as that of donepezil. Also, compound **(22)** involved in active binding site interactions with peripheral anionic site residues and extending into the deep gorge of a catalytic active site similar to donepezil. The detailed docking interaction analysis comparing the results

Table 6
Reversal of scopolamine-induced amnesia by the synthesized derivatives in the rat passive avoidance test.

Treatment {Dose(mg/kg)}	Entry latency (s)		
	Training trial	Retention trial	Δ
Control	17.83 ± 0.60	95.50 ± 0.76	77.67
SCP (1.5)	20.00 ± 0.63	35.17 ± 0.60[a]	15.17
12 (5.0) + SCP (1.5)	18.50 ± 0.76	57.83 ± 0.70[b]	39.33
12 (10.0) + SCP	19.17 ± 0.60	66.33 ± 0.49[b]	47.16
18 (5.0) + SCP	21.00 ± 0.63	89.83 ± 0.60[b]	68.83
18 (10.0) + SCP	20.33 ± 0.80	84.83 ± 0.60[b]	64.5
21 (5.0) + SCP	20.83 ± 0.60	82.17 ± 0.60[b]	61.34
21 (10.0) + SCP	20.17 ± 0.60	86.33 ± 0.66[b]	66.16
22 (5.0) + SCP	19.50 ± 0.76	90.17 ± 0.60[b]	70.67
22 (10.0) + SCP	16.67 ± 0.49	98.00 ± 0.63[b]	81.33
Donepezil (5.0) + SCP	19.00 ± 0.63	89.83 ± 0.60[b]	70.83
Donepezil (10.0) + SCP	17.17 ± 0.60	97.67 ± 0.49[b]	80.5

Data shown are expressed as mean ± SEM (n = 6).
Data were statistically analyzed by one-way ANOVA.
[a] Significantly different from control $p < 0.05$.
[b] Significantly different from the scopolamine-treated group $p < 0.05$; SCP = Scopolamine; Δ = Difference between retention trial and training trial.

Table 7
Effect of active semicarbazones of PABA on AChE activity in different regions of the rat brain.

Treatment {Dose(mg/kg)}	'n' moles of substrate hydrolyzed/min/mg protein		
	Prefrontal cortex	Hippocampus	Hypothalamus
Control	46.56 ± 0.66	48.68 ± 0.49	42.28 ± 0.60
12 (5.0	33.78 ± 0.94*	34.84 ± 0.49*	30.74 ± 0.42*
12 (10.0)	30.85 ± 0.47*	32.96 ± 0.57*	28.68 ± 0.66*
18 (5.0)	33.25 ± 0.55*	34.35 ± 0.66*	30.25 ± 0.42*
18 (10.0)	30.18 ± 0.47*	32.38 ± 0.98*	28.14 ± 0.60*
21 (5.0)	32.68 ± 0.57*	33.84 ± 0.47*	29.82 ± 0.42*
21 (10.0)	29.85 ± 0.42*	31.96 ± 0.90*	27.68 ± 0.60*
22 (5.0)	32.12 ± 0.49*	33.18 ± 0.49*	29.28 ± 0.66*
22 (10.0)	29.24 ± 0.42*	31.36 ± 0.76*	27.24 ± 0.60*
Donepezil (5.0)	31.25 ± 0.42*	32.38 ± 0.60*	28.54 ± 0.49*
Donepezil (10.0)	28.24 ± 0.76*	30.86 ± 0.60*	26.82 ± 0.57*

Data are expressed as mean ± SEM (n = 6). Data were statistically analyzed by one-way ANOVA.
* $p < 0.05$ compared to the control.

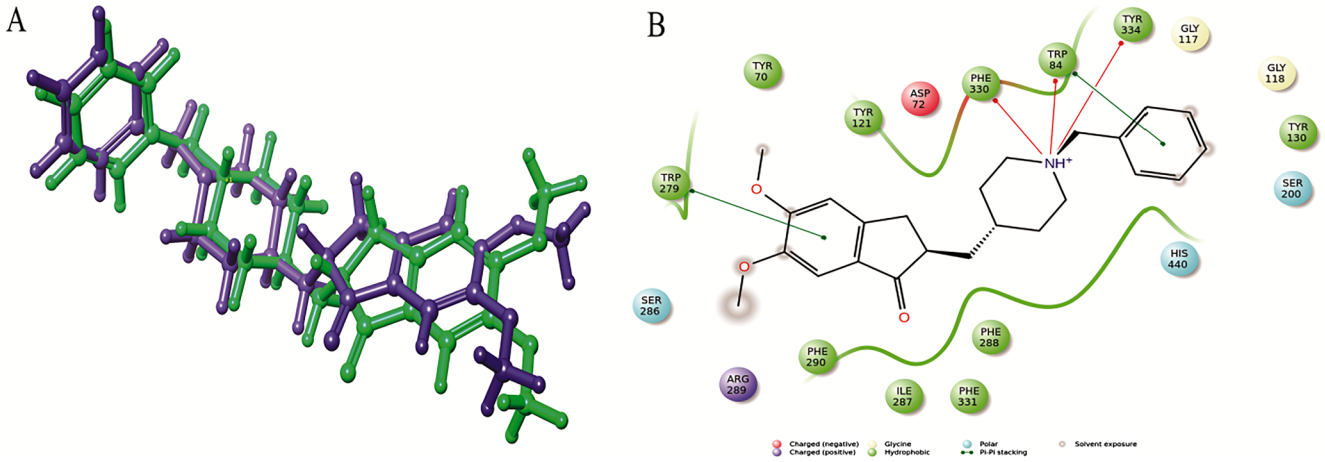

Fig. 3. Illustration of re-docking of co-crystallized structure and validation of docking protocols. (A) Superposition of co-crystallized structure of donepezil (Blue color) on the re-docked structure of donepezil (green color); (B) 2D interaction analysis of the re-docked structure of donepezil matching with the co-crystallized structure.

of compound **(22)** and donepezil is given in Table 8.

2.6. Molecular dynamics simulations

The binding pose stability of **(22)** AChE docked complex was affirmed by *in silico* molecular dynamics simulations. The overall stability of protein and ligand was evaluated with respect to the initial protein backbone structure using RMSD, and the results suggested that protein and ligand structure have remained energetically in stable trajectories with fluctuations within 3 Å (Fig. 5).

Further, interaction analysis of protein-ligand complex was evaluated through graphical charts and interaction fractions analysis. The interaction fractions provided the percentage of contacts maintained. The results of interaction fractions revealed that interactions which were observed with the active site residues in docking analysis were found to stable throughout the molecular dynamics simulation run of 50 ns (see Fig. 6).

3. Conclusions

A series of novel derivatives of PABA derivatives were computationally designed and synthesized as a potential cholinesterase inhibitor. The good statistical values obtained from the field based QSAR model (R^2 = 0.7972 for the training set, Q^2 = 0.7135, R_2CV = 0.5429, and Pearson-R = 0.8491). The synthesized derivatives were evaluated for their *in vitro* studies, where most of the compounds exhibited significant inhibitory potential against AChE and BChE. The top four compounds from AChE inhibition assay were further evaluated by *in vivo* animal models, where the hydroxyl-substituted compound **(22)** demonstrated significant activity comparable to standard donepezil. The *ex vivo* study confirmed the ability of the compound **(22)** to cross the blood-brain barrier, while the *in silico* studies demonstrated its mode of binding at active pocket in a stable manner. Thus, overall experimental studies suggested that the most promising compound **(22)** requires further development due to its promising *in vitro, in vivo, in silico*, and *ex vivo* results.

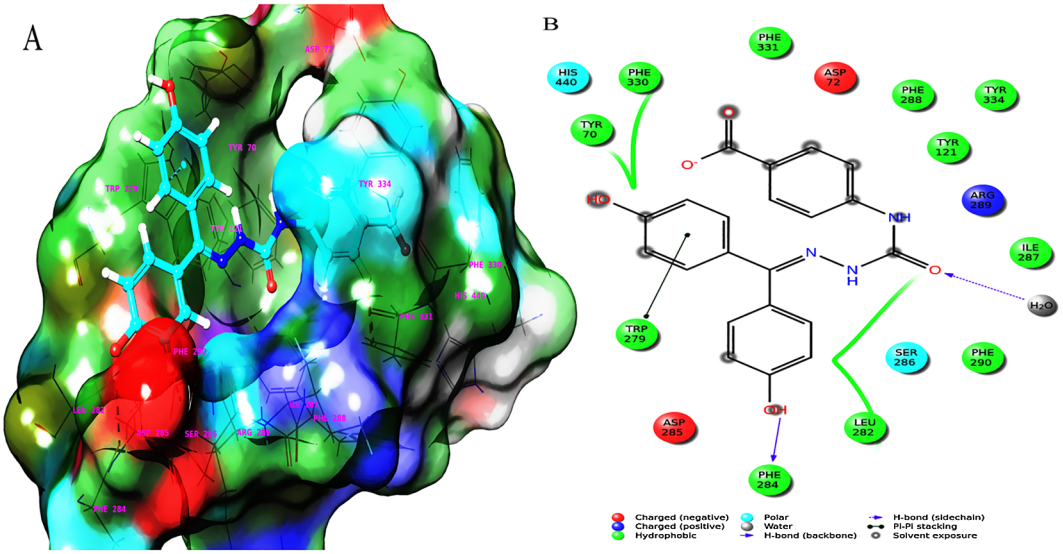

Fig. 4. Schematic representation of docking analysis of compound 22 on AChE (PDB Code: 1EVE). (A) 3D structural representation of docked complex of protein with compound 22 showing important active site interactions with polar (sky blue color), charged (blue and red color), and hydrophobic (green color) interactions; (B) 2D interaction analysis of compound 22 with AChE protein.

Table 8
Detailed comparative interaction analysis of compound (22) and donepezil on AChE.

Comp.	Interacting residues[#]				
	Catalytic site	Peripheral anionic site	Anionic subsite	Acyl binding pocket	Other interacting residues
22	Ser200[a], His440[a]	Tyr70[c], Asp72[d], Tyr121[c], Trp279[b,c],Tyr334[c],	Phe330[c]	Phe288[c], Phe290[c], Phe331[c]	Leu282[c], Phe284[e], Ser286[a], Ile287[c], Arg289[d], Phe331[c], Tyr334[c]
Don[*]	Ser200[a], His440[a]	Tyr70[c], Asp72[d], Tyr121[c], Trp279[b,c], Tyr334[c],	Trp84[b,f], Phe330[f]	Phe288[c], Phe290[c], Phe331[c]	Gly117[g], Gly118[g], Tyr130[c], Ser286[a], Ile287[c], Arg289[d], Phe331[c], Tyr334[c]

[#] All the interacting residues are within the 4 Å distance with the ligand.
[*] Don – Donepezil.
[a] Polar interaction.
[b] π-π stacking interaction.
[c] Hydrophobic interaction.
[d] Charged interaction.
[e] H-bonding interaction.
[f] π-π cation interaction.
[g] Glycine interaction.

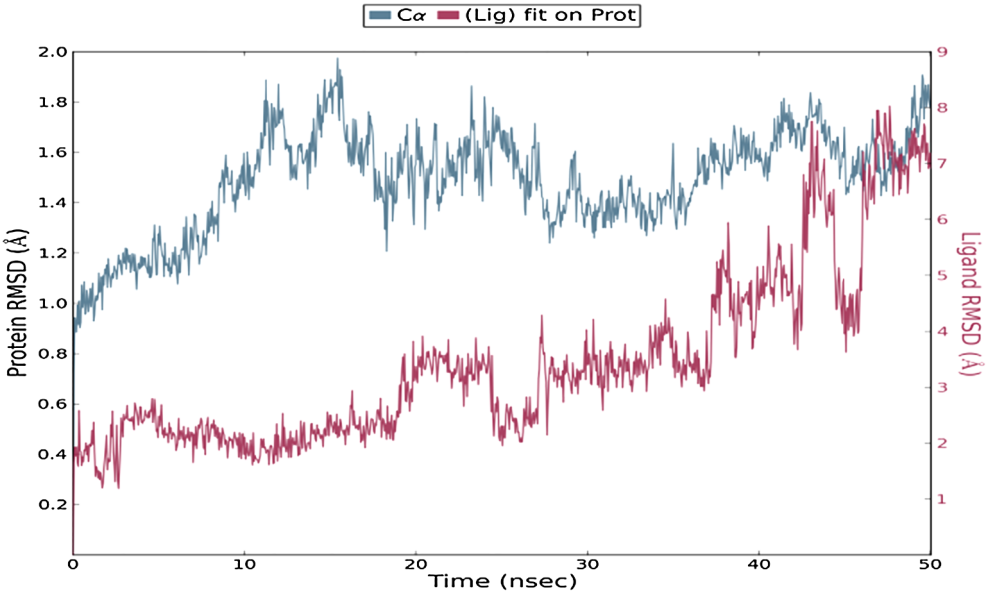

Fig. 5. RMSD measurement of protein and ligand structures concerning the initial protein backbone.

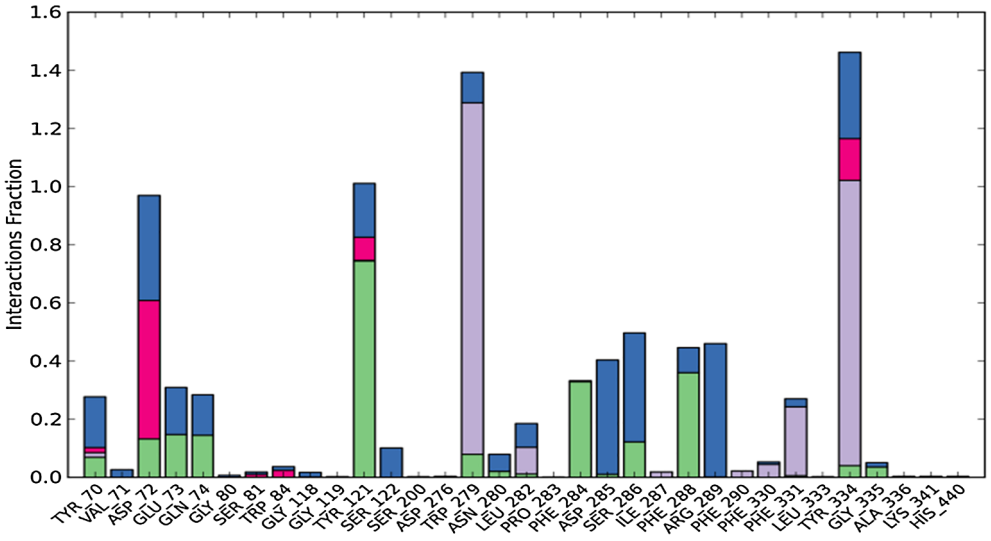

Fig. 6. Stacked bar chart analysis is representing protein-ligand interaction fractions.

4. Experimental section

4.1. Field-based 3D QSAR (FQSAR)

4.1.1. Compound selection and dataset preparation

A set comprising of 32 molecules reported from our previous reports were used for the field based QSAR analysis [16,35,36]. The field-based QSAR tool was employed to generate a 3D-QSAR model by randomly dividing the data set into 80% training set and 20% test set. The selected compounds have significant variations in the structure and their potency profiles. The IC_{50} values of the selected compounds varying from 0.052 μM to 274.3 μM. The IC_{50} values were converted into the pIC_{50} using the following formula as given below prior to QSAR model elaboration.

$$pIC_{50} = -\log_{10}(IC_{50})$$

All the compounds and their respective activities are listed in Supplementary Table S1, the 3D structures of all the ligands were generated using the builder panel of Maestro editor (Maestro, Schrodinger, LLC, New York, NY) and prepared with the LigPrep module (LigPrep, Schrödinger, LLC, New York, NY). Partial atomic charge and possible ionization states were generated at pH 7.0 using Epik module. Energy minimization of all sketched ligands was performed using the OPLS force field, and the resulting structures were used for the QSAR modeling.

4.1.2. Field-based QSAR

Field-based QSAR tool of Schrödinger 2018-1 was used for generating the Gaussian-based QSAR model. Using the Gaussian-based electrostatic, steric, hydrophobic, HBD, and HBA potential fields, the calculations were performed for QSAR modeling. For the developing of the QSAR model, 80% of the dataset molecules were randomly selected for the training set. Further, using the test set, the ligand activity model was validated. For the partial least square regression (PLS) analysis, pIC50 values of the molecules were used as the dependent variable, and Gaussian intensities were considered as an independent variable to derive the 3D-QSAR model. The QSAR model was built and calculated by constructing the 3D cubic lattice with 1 Å grid spacing and can be extended up to 3 Å beyond the training set limit with PLS factor of 5. Energy cutoff was set to ± 30 kcal/mol, and the variable with a standard deviation of < 0.01 was eliminated [37]. The five models were generated, and the best model was selected on the basis of statistical robustness. Further, 3D contour maps were generated using QSAR visualization module of the Maestro.

4.1.3. QSAR model validation

The stability and predictive power of the generated models were evaluated by using leave one out (LOO) cross-validation method. The statistical robustness was used to select the best model. The model was validated by the external test set compound using the crucial parameters of the test set include RMSE, Q^2, and Pearson-R that indicated the predictive ability of the model. The scattered plot was generated by correlating the observed and predictive activity of the data set molecules. The generated fields were then displayed as contour maps.

4.2. Chemistry

All reagents and solvents were procured from Sigma-Aldrich (India). The standard donepezil was obtained as a gift sample from Cipla Ltd., Maharashtra, India. The melting points (m.p.) of PABA derivatives were observed in open capillary tubes by a BI 9300 Bumstead/Electrothermal Stuart (SMPIO) melting point apparatus and reported as uncorrected. The reaction progress was observed by thin layer chromatography (TLC) on TLC silica gel 60 F254 aluminum sheets (Merck, India). FT-IR spectra were recorded on a Shimadzu FT-IR 8400S spectrophotometer at the scanning range 400–4000 cm^{-1}. ^1H NMR (500 MHz) and ^{13}C NMR (125 MHz) spectra were recorded on a Bruker Avance FT-NMR spectrometer in DMSO-d_6 using tetramethylsilane (TMS) as an internal standard. Chemical shift values were expressed in parts per million (δ). Elemental analyses were recorded by an Exeter CE-440 elemental analyzer.

4.2.1. General procedure

4.2.1.1. Synthesis of 4-(ethoxycarbonylamino) benzoic acid ***(2)*** *[38].* 4-aminobenzoic acid **(1)** (0.14 mol) was suspended in 1,4-dioxane/water (1:1, 100 ml), followed by addition of 1 M sodium hydroxide (100 ml) at 0–10 °C. Then, ethyl chloroformate (0.17 mol) was added slowly drop-wise into the mixture at 0–4 °C and stirred for overnight. The mixture was maintained up to pH 2.0 with 1 M aqueous hydrochloric acid (HCl). The reaction mixture was dissolved in the ethyl acetate (2 × 200 ml) and washed with 1 M HCl (100 ml), brine (2 × 100 ml). The ethyl acetate phase was distilled to get a gummy product. Further, the residue was purified by column chromatography on 100–200 mesh size silica gel phase by using mobile phase Ethyl acetate: Hexane (10:90) to get a white powder 4-(ethoxycarbonylamino)benzoic acid **(2)**.

Yield: 92.6%, ^1H NMR (500 MHz, δ_H ppm, DMSO-d_6): 1.28 (t, J = 6.4 Hz, 3H, CH_3), 4.16 (q, J = 6.2 Hz, 2H, CH_2), 7.58 (d, J = 8.6 Hz, 2H, Ar−H), 8.16 (d, J = 8.6 Hz, 2H, Ar−H), 12.12 (s, 1H, NH), 12.38 (s, 1H, COOH); ^{13}C NMR (125 MHz, δ_C ppm, DMSO-d_6): 16.8, 58.4, 118.2, 118.2, 130.1, 130.7, 131.2, 145.8, 157.5, 169.2.

4.2.1.2. Synthesis of 4-(hydrazinecarboxamido)benzoic acid ***(3)*** *[39].* Compound **(2)** (0.047 mol), and hydrazine hydrate ($N_2H_4{\cdot}H_2O$) (0.24 mol) was suspended in the dried ethanol and refluxed for 2–3 h. On the completion of the reaction the solvent was evaporated under vacuum to get the crude compound **(3)**.

Yield: 82.9%, ^1H NMR (500 MHz, δ_H ppm, DMSO-d_6): 4.68 (s, 2H, NH_2), 5.46 (s, 1H, NH), 7.79 (d, J = 7.5 Hz, 2H, Ar−H), 8.22 (d, J = 7.5 Hz, 2H, Ar−H), 12.16 (s, 1H, NH), 12.46 (s, 1H, COOH); ^{13}C NMR (125 MHz, δ_C ppm, DMSO-d_6): 115.7, 115.8, 122.1, 128.7, 128.8, 142.7, 158.8, 166.9.

4.2.1.3. Synthesis of benzylidene (hydrazinecarboxamido)benzoic acid derivative ***(4–11)***. Compound **(3)** (0.01 mol) and equimolar quantities of variously substituted aldehydes (0.01 mol) were mixed in 95% ethanol (10 ml) with an acid catalyst. The solution was refluxed for 4–6 h and allowed to cool to afford the solid compounds **(4–11)**.

4.2.1.3.1. 4-(2-benzylidenehydrazine-1-carboxamido)benzoic acid ***(4)***. Yield: 85.2%, FT-IR (KBr, cm^{-1}): 1456 (C═C, Aromatic), 1624 (C═N), 1650 (C═O, NHCONH), 1703 (C═O, COOH), 3015 (═CH), 3430 (NH, NHCONH), 3510 (OH, COOH); ^1H NMR (500 MHz, δ_H ppm, DMSO-d_6): 7.34–8.21 (m, 10H, Ar−H, −N═CH−), 12.21 (brs, 2H, −NH) 12.46 (s, 1H, COOH); ^{13}C NMR (125 MHz, δ_C ppm, DMSO-d_6): 122.3, 126.7, 129.7, 130.8, 131.7, 132.8, 135.3, 141.3, 145.4, 159.2, 171.2; Anal. (%) for $C_{15}H_{13}N_3O_3$: C 63.60, H 4.63, N 14.83; found (%). C 63.55, H 4.61, N 14.85.

4.2.1.3.2. 4-(2-(2-hydroxybenzylidene)hydrazine-1-carboxamido) benzoic acid ***(5)***. Yield: 64.6%, FT-IR (KBr, cm^{-1}): 1460 (C═C, Aromatic), 1630 (C═N), 1650 (C═O, NHCONH), 1703 (C═O, COOH), 3015 (═CH, Aromatic), 3424 (NH, NHCONH), 3510 (OH, COOH), 3525 (OH, Phenolic); ^1H NMR (500 MHz, δ_H ppm, DMSO-d_6): 6.85–8.34 (m, 9H, Ar−H, −N═CH), 9.52 (s, 1H, −OH), 12.34 (brs, 2H, −NH), 12.52 (s, 1H, COOH); ^{13}C NMR (125 MHz, δ_C ppm, DMSO-d_6): 116.3, 119.3, 122.3, 126.7, 129.7, 130.8, 132.8, 142.3, 145.3, 159.4, 162.2, 171.4; Anal. (%) for $C_{15}H_{13}N_3O_4$: C 63.60, H 4.63, N 14.83; found (%) C 63.65, H 4.66, N 14.78.

4.2.1.3.3. 4-(2-(2,4-dihydroxybenzylidene)hydrazine-1-carboxamido) benzoic acid ***(6)***. Yield: 75.8%, FT-IR (KBr, cm-1): 1465 (C═C, Aromatic), 1612 (C═N), 1650 (C═O, NHCONH), 1703 (C═O, COOH), 3015 (═CH, Aromatic), 3410 (NH, NHCONH), 3510 (OH, COOH), 3525 (OH, Phenolic); ^1H NMR (500 MHz, δ_H ppm, DMSO-d_6):

6.65–8.25 (m, 8H, Ar—H, —N=CH), 9.63 (s, 2H, OH), 12.34 (brs, 2H, —NH), 12.52 (s, 1H, COOH); ^{13}C NMR (125 MHz, δ_C ppm, DMSO-d_6): 109.3, 111.3, 122.7, 126.7, 130.8, 132.8, 142.3, 145.4, 159.2, 162.6, 163.1, 171.2; Anal. (%) for $C_{15}H_{13}N_3O_5$: C 57.14, H 4.16, N 13.33; found (%). C 57.18, H 4.15, N 13.31.

4.2.1.3.4. 4-(2-(2,4,6-trihydroxybenzylidene)hydrazine-1-carboxamido)benzoic acid (7). Yield: 68.4%, FT-IR (KBr, cm^{-1}): 1470 (C=C, Aromatic), 1628 (C=N), 1650 (C=O, NHCONH), 1703 (C=O, COOH), 3015 (=CH, Aromatic), 3421 (NH, NHCONH), 3510 (OH, COOH), 3525 (OH, Phenolic); ^{1}H NMR (500 MHz, δ_H ppm, DMSO-d_6): 6.67–8.23 (m, 7H, Ar—H, —N=CH), 9.68 (s, 3H, OH), 12.23 (brs, 2H, —NH), 12.59 (s, 1H, COOH), ^{13}C NMR (125 MHz, δ_C ppm, DMSO-d_6): 97.6, 106.2, 122.3, 126.7, 130.8, 142.8, 145.2, 159.2, 164.6, 165.1, 171.2; Anal. (%) for $C_{15}H_{13}N_3O_6$: C 54.38, H 3.96, N 12.68; found (%). C 54.35, H 3.95, N 12.66.

4.2.1.3.5. 4-(2-(2-methoxybenzylidene)hydrazine-1-carboxamido) benzoic acid (8). Yield: 72.8%, FT-IR (KBr, cm^{-1}): 1456 (C=C, Aromatic), 1607 (C=N), 1650 (C=O, NHCONH), 2905 (CH, CH_3), 3015 (=CH, Aromatic), 1703 (C=O, COOH), 3329 (NH, NHCONH), 3512 (OH, COOH); ^{1}H NMR (500 MHz, δ_H ppm, DMSO-d_6): 3.84 (s, 3H, $-OCH_3$), 7.10–8.23 (m, 9H, Ar—H, —N=CH), 12.23 (brs, 2H, —NH), 12.58 (s, 1H, COOH); ^{13}C NMR (125 MHz, δ_C ppm, DMSO-d_6): 58.6, 115.0, 117.3, 122.3, 126.7, 130.7, 131.5, 132.7, 142.3, 145.4, 159.1, 162.8, 171.6; Anal. (%) for $C_{16}H_{15}N_3O_4$: C 61.34, H 4.83, N 13.41; found (%) C 61.28, H 4.8, N 13.40.

4.2.1.3.6. 4-(2-(2,4-dimethoxybenzylidene)hydrazine-1-carboxamido) benzoic acid (9). Yield: 74.6%, FT-IR (KBr, cm^{-1}): 1456 (C=C, Aromatic), 1599 (C=N), 1650 (C=O, NHCONH), 1703 (C=O, COOH), 2905 (CH, CH_3), 3015 (=CH, Aromatic), 3326 (NH, NHCONH), 3509 (OH, COOH); ^{1}H NMR (500 MHz, δ_H ppm, DMSO-d_6): 3.80 (s, 6H, $-OCH_3$), 7.01–8.21 (m, 8H, Ar—H, —N=CH), 12.22 (brs, 2H, —NH), 12.55 (s, 1H, COOH); ^{13}C NMR (125 MHz, δ_C ppm, DMSO-d_6): 58.2, 105.0, 108.2, 111.3, 122.3, 126.6, 131.8, 132.6, 142.6, 145.4, 159.2, 162.2,162.9, 171.5; Anal. (%) for $C_{17}H_{17}N_3O_5$: C 59.47, H 4.99, N 12.24; found (%) C 59.42, H 4.97, N12.22.

4.2.1.3.7. 4-(2-(2,4,6-trimethoxybenzylidene)hydrazine-1-carboxamido)benzoic acid (10). Yield: 66.2%, FT-IR (KBr, cm^{-1}): 1456 (C=C, Aromatic), 1621 (C=N), 1650 (C=O, NHCONH), 1703 (C=O, COOH), 2905 (CH, CH_3), 3015 (=CH, Aromatic), 3345 (NH, NHCONH), 3508 (OH, COOH); ^{1}H NMR (500 MHz, δ_H ppm, DMSO-d_6): 3.86 (s, 9H, OCH_3), 6.86–8.17 (m, 7H, Ar—H, —N=CH), 12.26 (brs, 2H, —NH), 12.56 (s, 1H, COOH); ^{13}C NMR (125 MHz, δ_C ppm, DMSO-d_6): 58.3, 93.6, 103.3, 122.2, 126.7, 131.4, 142.3, 145.4, 159.5, 162.3, 162.6, 171.5; Anal. (%) for $C_{18}H_{19}N_3O_6$: C 57.90, H 5.13, N 11.25; found (%) C 57.92, H 5.11, N 11.24.

4.2.1.3.8. 4-(2-(4-hydroxy-3,5-dimethoxybenzylidene)hydrazine-1-carboxamido)benzoic acid (11). Yield: 68.4%, FT-IR (KBr, cm^{-1}): 1456 (C=C, Aromatic), 1624 (C=N), 1650 (C=O, NHCONH), 1703 (C=O, COOH), 2905 (CH, CH_3), 3015 (=CH, Aromatic), 3375 (NH, NHCONH), 3510 (OH, COOH), 3530 (OH, Phenolic); ^{1}H NMR (500 MHz, δ_H ppm, DMSO-d_6): 3.86 (s, 6H, $-OCH_3$), 6.79–8.11 (m, 7H, Ar—H, —N=CH), 9.65 (s, 1H, OH), 12.26 (brs, 2H, —NH), 12.58 (s, 1H, COOH); ^{13}C NMR (125 MHz, δ_C ppm, DMSO-d_6): 58.6, 110.3, 122.3, 126.5, 129.3, 131.7, 135.8, 142.3, 145.4, 158.2, 162.4, 171.2; Anal. (%) for $C_{17}H_{17}N_3O_6$: C 56.82, H 4.77, N 11.69; found (%). C 56.86, H 4.75, N 11.67.

4.2.1.4. Synthesis of 4-(2-(bis(phenyl)methylene)hydrazinecarboxamido) benzoic acid derivative (12–23). Compound 3 (0.01 mol), substituted benzophenone (0.01 mol) and activated molecular sieves 4A was added in benzene (10 ml) at room temperature for 20 min to get the precipitate of the compound. The absolute ethanol was added to dissolve the suspension, filtered, and molecular sieves were separated. The filtrate was evaporated under reduced pressure to get the crude compound, which was further purified by column chromatography on 100–200 mesh size silica gels with mobile phase DCM: Methanol (9:1) to get a white powder.

4.2.1.4.1. 4-(2-(1-phenylethylidene)hydrazine-1-carboxamido)benzoic acid (12). Yield: 81.2%, FT-IR (KBr, cm^{-1}): 1450 (C=C, Aromatic), 1625 (C=N), 1650 (C=O, NHCONH), 1703 (C=O, COOH), 2910 (CH, CH3), 3015 (=CH, Aromatic), 3431 (NH, NHCONH), 3512 (OH, COOH), ^{1}H NMR (500 MHz, δ_H ppm, DMSO-d_6): 2.37 (s, 3H, $-CH_3$), 7.31–7.78 (m, 9H, Ar—H), 12.48 (brs, 2H, —NH), 12.65 (s, 1H, COOH); ^{13}C NMR (125 MHz, δ_C ppm, DMSO-d_6): 13.6, 122.3, 126.7, 129.1, 130.8, 131.4, 134.6, 142.3, 159.2, 162.8, 171.9, Anal. (%) for $C_{16}H_{15}N_3O_3$: C 64.64, H 5.09, N 14.13; found (%) C 64.55, H 5.11, N 14.11.

4.2.1.4.2. 4-(2-(1-(4-methoxyphenyl)ethylidene)hydrazine-1-carboxamido)benzoic acid (13). Yield: 81.8%, FT-IR (KBr, cm^{-1}): 1456 (C=C, Aromatic), 1615 (C=N), 1650 (C=O, NHCONH), 1703 (C=O, COOH), 2915 (CH, CH_3), 3015 (=CH, Aromatic), 3405 (NH, NHCONH), 3515 (OH, COOH); ^{1}H NMR (500 MHz, δ_H ppm, DMSO-d_6): 2.55 (s, 3H, $-CH_3$), 3.81 (s, 3H, $-OCH_3$), 6.85–8.10 (m, 8H, Ar—H), 12.41 (brs, 2H, —NH), 12.62 (brs, 1H, COOH); ^{13}C NMR (125 MHz, δ_C ppm, DMSO-d_6): 21.6, 58.3, 115.1, 122.3, 126.3, 127.7, 130.1, 134.8, 142.3, 159.2, 162.9, 163.2,171.2; Anal. (%) for $C_{17}H_{17}N_3O_4$: C 62.38, H 5.23, N 12.84; found (%) C 62.34, H 5.22, N 12.86.

4.2.1.4.3. 4-(2-(1-(4-hydroxy-3-methoxyphenyl)ethylidene)hydrazine-1-carboxamido)benzoic acid (14). Yield: 80.2%, FT-IR (KBr, cm^{-1}): 1456 (C=C, Aromatic), 1630 (C=N), 1650 (C=O, NHCONH), 1703 (C=O, COOH), 2905 (CH, CH_3), 3015 (=CH, Aromatic), 3387 (NH, NHCONH), 3510 (OH, COOH), 3525 (OH, Phenolic); ^{1}H NMR (500 MHz, δ_H ppm, DMSO-d_6): 2.34 (m, 3H, $-CH_3$), 3.84 (s, 3H, $-OCH_3$), 6.69–8.11 (m, 7H, Ar—H), 9.86 (s, 1H, —OH), 12.42 (brs, 2H, —NH), 12.60 (brs, 1H, COOH); ^{13}C NMR (125 MHz, δ_C ppm, DMSO-d_6): 21.1, 56.2, 115.1, 117.8, 122.1, 123.1, 126.3, 128.5, 131.8, 142.4, 148.3, 152.1, 159.1, 162.5, 171.2; Anal. (%) for $C_{17}H_{17}N_3O_5$: C 59.47, H 4.99, N 12.24; found (%) C 59.42, H 4.98, N 12.21.

4.2.1.4.4. 4-(2-(1-phenylpropylidene)hydrazine-1-carboxamido) benzoic acid (15). Yield: 86.5%, FT-IR (KBr, cm^{-1}): 1456, 1500 (C=C, Aromatic), 1590 (C=N), 1650 (C=O, NHCONH), 1703 (C=O, COOH), 2905 (CH, CH_3), 3015 (=CH, Aromatic), 3432 (NH, NHCONH), 3512 (OH, COOH); ^{1}H NMR (500 MHz, δ_H ppm, DMSO-d_6): 0.90 (m, 2H, $-CH_2$), 1.33 (m, 3H, $-CH_3$), 7.34–7.81 (m, 9H, Aromatic-H), 12.45 (brs, 2H, —NH), 12.71 (brs, 1H, COOH); ^{13}C NMR (125 MHz, δ_C ppm, DMSO-d_6): 12.9, 29.6, 122.5, 126.2, 129.4, 130.8, 131.3, 132.8, 135.3, 142.3, 162.2, 162.8, 171.3; Anal. (%) for $C_{17}H_{17}N_3O_3$: C 65.58, H 5.50, N 13.50; found (%) C 65.52, H 5.51, N 13.52.

4.2.1.4.5. 4-(2-(1-(4-methoxyphenyl)propylidene)hydrazine-1-carboxamido)benzoic acid (16). Yield: 88.2%, FT-IR (KBr, cm^{-1}): 1456, 1500 (C=C, Aromatic), 1597 (C=N), 1650 (C=O, NHCONH), 1703 (C=O, COOH), 2905 (CH, CH_3), 3015 (=CH, Aromatic), 3413 (NH, NHCONH), 3514 (OH, COOH); ^{1}H NMR (500 MHz, δ_H ppm, DMSO-d_6): 0.93 (m, 2H, $-CH_2$), 1.33 (m, 3H, $-CH_3$), 3.69 (s, 3H, $-OCH_3$), 6.84–8.12 (m, 8H, Ar—H), 12.36 (brs, 2H, —NH), 12.59 (brs, 1H, COOH); ^{13}C NMR (125 MHz, δ_C ppm, DMSO-d_6): 12.2, 28.2, 58.5, 115.1, 122.7, 126.1, 127.2, 131.8, 132.1, 142.3, 159.2, 162.6, 162.9, 171.6; Anal. (%) for $C_{18}H_{19}N_3O_4$: C 63.33, H 5.61, N 12.31; found (%) C 63.36, H 5.62, N 12.33.

4.2.1.4.6. 4-(2-(1-(4-hydroxy-3-methoxyphenyl)propylidene) hydrazine-1-carboxamido)benzoic acid (17). Yield: 76.5%, FT-IR (KBr, cm^{-1}): 1456, 1500 (C=C, Aromatic), 1627 (C=N), 1650 (C=O, NHCONH), 1703 (C=O, COOH), 2905 (CH, CH_3), 3015 (=CH, Aromatic), 3423 (NH, NHCONH), 3512 (OH, COOH), 3525 (OH, Phenolic); ^{1}H NMR (500 MHz, δ_H ppm, DMSO-d_6): 0.90 (m, 2H, $-CH_2$) 1.32 (m, 3H, $-CH_3$), 3.86 (s, 3H, $-OCH_3$), 6.67–8.01 (m, 7H, Ar—H), 9.81 (s, 1H, —OH), 12.41 (brs, 2H, —NH), 12.61 (brs, 1H, COOH); ^{13}C NMR (125 MHz, δ_C ppm, DMSO-d_6): 12.1, 28.1, 57.2, 115.1, 117.3, 122.3, 126.7, 127.7, 128.2, 129.7, 131.4, 142.3, 148.4, 152.2, 162.2, 162.6, 171.5; Anal. (%) for $C_{18}H_{19}N_3O_5$: C 60.50, H 5.36,

N 11.76; found (%). C 60.55, H 5.34, N 11.78.

*4.2.1.4.7. 4-(2-(diphenylmethylene)hydrazine-1-carboxamido)benzoic acid (**18**).* Yield: 78.6%, FT-IR (KBr, cm^{-1}): 1456, 1500 (C═C, Aromatic), 1615 (C═N), 1650 (C═O, NHCONH), 1703 (C═O, COOH), 3015 (═CH, Aromatic), 3354 (NH, NHCONH), 3511 (OH, COOH); ^{1}H NMR (500 MHz, δ_H ppm, DMSO-d_6): 7.34–7.83 (m, 14H, Ar−H), 12.32 (brs, 2H, −NH), 12.61 (brs, 1H, COOH); ^{13}C NMR (125 MHz, δ_C ppm, DMSO-d_6): 122.3, 126.6, 128.3, 129.8, 130.8, 131.8, 133.6, 142.3, 156.2, 162.6, 171.3; Anal. (%) for $C_{21}H_{17}N_3O_3$: C 70.18, H 4.77, N 11.69; found (%) C 70.15, H 4.76, N 11.67.

*4.2.1.4.8. 4-(2-((4-methoxyphenyl)(phenyl)methylene)hydrazine-1-carboxamido)benzoic acid (**19**).* Yield: 82.8%, FT-IR (KBr, cm^{-1}): 1456, 1500 (C═C, Aromatic), 1611 (C═N), 1650 (C═O, NHCONH), 1703 (C═O, COOH), 2905 (CH, CH_3), 3015 (═CH, Aromatic), 3356 (NH, NHCONH), 3511 (OH, COOH), ^{1}H NMR (500 MHz, δ_H ppm, DMSO-d_6): 3.84 (s, 3H, OCH_3), 6.98–7.98 (m, 13H, Ar−H), 12.41 (brs, 2H, −NH), 12.66 (brs, 1H, COOH); ^{13}C NMR (125 MHz, δ_C ppm, DMSO-d_6): 56.7, 115.3, 122.3, 125.3, 126.7, 128.2, 129.5, 130.1, 131.8, 133.3, 142.1, 156.2, 162.2, 163.3, 171.5; Anal. (%) for $C_{22}H_{19}N_3O_4$: C 67.86, H 4.92, N 10.79; found (%). C 67.82, H 4.91, N 10.78.

*4.2.1.4.9. 4-(2-(bis(4-methoxyphenyl)methylene)hydrazine-1-carboxamido)benzoic acid (**20**).* Yield: 68.4%, FT-IR (KBr, cm^{-1}): 1456, 1500 (C═C, Aromatic), 1621 (C═N), 1650 (C═O, NHCONH), 1703 (C═O, COOH), 3015 (═CH, Aromatic), 3389 (NH, NHCONH), 3512 (OH, COOH); ^{1}H NMR (500 MHz, δ_H ppm, DMSO-d_6): 3.81 (s, 6H, $-OCH_3$), 6.89–7.97 (m, 12H, Ar−H), 12.41 (brs, 2H, −NH), 12.67 (brs, 1H, COOH); ^{13}C NMR (125 MHz, δ_C ppm, DMSO-d_6): 56.6, 115.1, 122.2, 125.3, 126.6, 130.1, 131.6, 142.4, 163.1, 163.4, 156.1, 171.6, Anal. (%) for $C_{23}H_{21}N_3O_5$: C 65.86, H 5.05, N 10.02; found (%) C 65.80, H 5.05, N 10.04.

*4.2.1.4.10. 4-(2-((4-hydroxyphenyl)(phenyl)methylene)hydrazine-1-carboxamido)benzoic acid (**21**).* Yield: 86.2%, FT-IR (KBr, cm^{-1}): 1456, 1500 (C═C, Aromatic), 1594 (C═N), 1650 (C═O, NHCONH), 1703 (C═O, COOH), 3015 (═CH, Aromatic), 3401 (NH, NHCONH), 3509 (OH, COOH), 3525 (OH, Phenolic); ^{1}H NMR (500 MHz, δ_H ppm, DMSO-d_6): 6.82–7.86 (m, 13H, Ar−H), 9.87 (s, 1H, −OH), 12.36 (brs, 2H, −NH), 12.62 (brs, 1H, COOH); ^{13}C NMR (125 MHz, δ_C ppm, DMSO-d_6): 116.0, 122.3, 125.1, 126.3, 128.7, 129.3, 130.0, 131.7, 133.3, 142.3, 156.7, 162.4, 163.2, 171.2; Anal. (%) for $C_{21}H_{17}N_3O_4$: C 67.19, H 4.56, N 11.19; found (%) C 67.15, H 4.55, N 11.18.

*4.2.1.4.11. 4-(2-(bis(4-hydroxyphenyl)methylene)hydrazine-1-carboxamido)benzoic acid (**22**).* Yield: 80.6%, FT-IR (KBr, cm^{-1}): 1650 (C═O, NHCONH), 1703 (C═O, COOH), 3015 (═CH, Aromatic), 3301 (NH, NHCONH), 3515 (OH, COOH), 3525 (OH, Phenolic); ^{1}H NMR (500 MHz, δ_H ppm, DMSO-d_6): 6.87 (d, J = 8.5 Hz, 2H, Ar−H), 7.56–7.61 (m, 6H, Ar−H), 7.85–7.87 (d, J = 8.5 Hz, 4H, Ar−H), 10.00 (s, 2H, −OH), 12.56 (brs, 2H, −NH); ^{13}C NMR (125 MHz, δ_C ppm, DMSO-d_6): 115.4, 117.7, 124.7, 129.2, 130.9, 132.4, 143.9, 153.8, 161.7, 167.4; Anal. (%) for $C_{21}H_{17}N_3O_5$: C 64.45, H 4.38, N 10.74; found (%) C 64.40, H 4.38, N 10.72.

*4.2.1.4.12. 4-(2-((2,4-dimethoxyphenyl)(4-hydroxyphenyl) methylene)hydrazine-1-carboxamido)benzoic acid (**23**).* Yield: 75.4%, FT-IR (KBr, cm^{-1}): 1456, 1500 (C═C, Aromatic), 1600 (C═N), 1650 (C═O, NHCONH), 1703 (C═O, COOH), 2904 (CH, CH_3), 3015 (═CH, Aromatic), 3430 (NH, NHCONH), 3512 (OH, COOH), 3525 (OH, Phenolic); ^{1}H NMR (500 MHz, δ_H ppm, DMSO-d_6): 3.71 (s, 3H, $-OCH_3$), 3.86 (s, 3H, $-OCH_3$), 6.82–7.86 (m, 11H, Aromatic−H), 9.89 (s, 1H, −OH), 12.38 (brs, 2H, −NH), 12.64 (brs, 1H, COOH); ^{13}C NMR (125 MHz, δ_C ppm, DMSO-d_6): 59.2, 61.1, 102.3, 107.0, 109.4, 116.3, 122.4, 125.2, 126.7, 131.8, 132.4, 142.3, 156.2, 159.6, 161.5, 162.4, 165.4, 171.2; Anal. (%) for $C_{23}H_{21}N_3O_6$: C 63.44, H 4.86, N 9.65; found (%) C 63.40, H 4.85, N 9.63.

4.3. Estimation of cholinesterase activity

The Ellman's spectrophotometric method of AChE (electric eel) and BChE (human serum) inhibition was used to determine the IC_{50} values of the selected compounds [40]. At 412 nm, an increase in absorbance was recorded for 5 min. The stock solution of AChE and BChE (lyophilized powder) were prepared by dissolving it in 0.1 M phosphate buffer pH 8.0. Final assay mixture consisted of 0.1 M phosphate buffer pH 8.0, 340 mM of 5,5′-dithiobis(2-nitrobenzoic acid), 550 mM of the substrate (acetylthiocholine iodide or butyrylthiocholine iodide), 0.02 unit/ml of AChE or BChE, and respective test compounds in varied concentration range. Inhibition of enzyme activity was measured by taking a 20–80% concentration of the selected compounds. The enzyme with the assay solution was subjected to incubation for 20 min at 37 °C followed by the addition of substrate. The percentage inhibition by increasing concentration of the compounds was determined by comparing the reaction rate to that of the blank assay values. The values were calculated in triplicates, and the IC_{50} values were expressed graphically as log concentration percent inhibition curves [41,42].

4.4. Enzyme kinetics study

The type of enzyme inhibition was determined by Ellman's spectrophotometric analysis. The inhibitory kinetics was determined with fixed cholinesterase concentration, acetylthiocholine iodide and butyrylthiocholine iodide in a different concentration below and above Km as a substrate in alternative sequence with phosphate buffer pH 8.0. The study was performed in the presence or absence of the different compounds. Lineweaver and Burk's method was used to evaluate the inhibitory kinetics, and the concentration of the compounds was kept approximate to the IC_{50} of enzyme inhibition [22].

4.5. Biological studies

4.5.1. Animals

In the experimental studies, 4–5 months old albino strain rats (Charles Foster rats) of 150–200 g of either sex were used. All animals were procured from Central Animal House, Institute of Medical Sciences, Banaras Hindu University, Varanasi (Registration No. 542/02/ab/CPCSEA) The semi-synthetic balanced diet, with occasionally supplied of green vegetables (scaled leaves) and water *ad libitum* were used to fed the animals. Animals were kept in cages (six rats in one cage) and conditions were maintained (temp. 22 ± 3 °C and 45–55% relative humidity). All animals were strictly exposed to dark and light cycles in the fully ventilated room. All necessary permissions were obtained from the Institutional Animal Ethical Committee (No. Dean/11-12/CAEC/329).

4.5.2. Acute toxicity evaluation

The acute toxicity of the compounds was determined following the OECD (4 2 3) guidelines. A 150–200 g nulliparous, non-pregnant, female albino rats were kept on fasting overnight before testing. On an experimental day, the compounds in graded dose up to 500 mg/kg p.o. were administered in 0.3% of carboxymethyl cellulose as a vehicle. The animals were observed in 30 min, 2 h, and up to 48 h for any behavioral or autonomic changes. The animals under study were also monitored for any kind of change in signs like convulsion, tremor, salivation, diarrhea, sleep, pulse rate, heart rate, B.P. and feeding behaviors that are related to acute toxicity. No mortality was observed for tested compound (**12, 18, 21 and 22**) indicated that these compounds could be tolerated at a maximum dose of 500 mg/kg p.o. suggested a significant margin of safety for all the tested compounds [43,44].

4.5.3. Drug treatment

The standard drug donepezil and the test compounds in 0.3% carboxymethylcellulose (suspension) were administered 5 mg/kg and 10 mg/kg once daily for 16 days. The control groups were treated with 0.3% of carboxymethyl cellulose equal to the volume of the experimental compounds (See Supplementary Table S6).

4.5.4. Morris water maze (MWM) task

The Morris water maze is a 45 cm deep and 120 cm in diameter semicircular metallic pool containing four equal quadrants. This pool is filled with water at approximately 25 cm in depth. At the center of the quadrant and below the 0.5 cm of an opaque surface, a platform of 15 cm in diameter submerged into a quadrant of the circular pool. This pool was then placed on the center of a small room (test room), which surrounded by the extra-maze cues. To provide both distal and proximal visual cues, many extra-maze cues was placed on the wall of the room and two on the rim of the pool. The rats under study (each rat from each group) are then placed into the water pool by hands facing the wall. The 60 s time was given to each rat to find out the platform and on successful completion, the next 20 s time was given to observe the spatial cues. In this particular time, the rats if not able to find out the platform need to be guided to reach the respective location. The episodes of animals were scored live by a blind observer included swim distance, escape latency, and time spent in the target quadrant [45,46].

4.5.5. Habituation

The albino rats used in the experiment were habituated to 60 s swim without platform pool. This was done just before 24 h of starting the training.

4.5.6. Spatial reference memory (SRM) testing in the water maze

SRM (special reference memory) testing was commenced on the 7th day of the treatment. One hour after the administration of the last dose of donepezil or compound. For the next three consecutive days (7–9th day), eight trials/day (10 min interval), for animals were carried out. In every trial, the animals in the pool were released from different point however the escape platform was fixed. The release point of the animal was the middle of the quadrant, and it was at the age of the pool. After completion of the test (7–9th day) on the 10th day, animals were placed into their home cages and were subjected to probe trial. In probe trial, a free swim period (without platform) of 60 s were recorded (live scoring).

4.5.7. Spatial working memory (SWM) testing in the water maze

In the reference memory test, eight trials were received by each rat every day. After the reference memory test, the subjected animals equipped for the working memory task [47]. On day 13, 48 h after initial testing pre-training phase, the working memory task was started. Over four consecutive days (13–16 days), two trials per day were given. In acquisition trial or first trial each day, rats had to find a platform at a new position (new task). After 75 m of the first trial, a retrieval trial or second trial was performed in which the platform was in its previous position, and the animals were started from one of the three possible locations different from preceding trials.

4.5.8. Passive avoidance task

The apparatus used for this task consisted of two identical light and dark compartments with grid floors that can be electrified separately and a guillotine door connecting the two compartments. During the training trial, rats were placed in the light compartment 10 s after placing the animals in the compartment the door was raised. As soon as the animal placed all four paws in the dark compartment, the door of the compartment closed automatically, and 0.02 mA/10 g body weight electrical foot shock lasting 2 s was then delivered. The training trial entry latency time was then recorded as the time elapsed from the placement of the rat in the light compartment until entry into the dark compartment. After 24 h of the training trial, a retention trial was performed following the similar procedure except for the electric shock and their entry to dark compartment measured. The standard drug (donepezil) and the test compounds in 0.3% carboxymethylcellulose (suspension) were administered orally 20 min prior to start a training session, and immediately after completion of the training session, injected an amnesic drug. In retention session the maximum allowed entry latency was 120 s [48,49].

4.5.9. Open-field test

To observe the locomotor activity in subjected animals the Open field test was carried out. In this test, animals were placed in a 15 * 30 * 38 cm wooden box with a 5 cm square grid marked on the floor and number of lines crossed by each animal at the frequency of 3 min was recorded [50].

4.5.10. Estimation of AChE activity in brain tissue

All the rats in experimental studies were sacrificed after an hour of administration of the last dose of compounds and donepezil. The specific parts of the brain namely the hippocampus, prefrontal cortex, and hypothalamus were isolated. The isolated brain portions were then homogenized in phosphate buffer (pH 8.0 and previously ice cold) in 1:10 ratio and subjected to centrifuge at 1000 rpm for 10 min at 4 °C. After centrifugation, the supernatant was collected and used as the enzyme source. Using 0.25 M isoOMPA (tetraisopropylpyrophoshoramide) the activity of BChE was blocked, and AChE activity was determined using standard spectrophotometric method (Ellman's method). The determined enzyme activity was expressed in 'n' mole/min/mg (protein substrate hydrolyzed/min/mg) [51].

4.6. Molecular docking studies

The docking experiment of compound **(22)** was performed on AChE enzyme using Glide module of Schrödinger Maestro 2018–1 MM Share Version. The stable conformers of compound **(22)** with minimum potential energy using an OPLS-2005 force field were generated. The structure of AChE (PDB Code: 1EVE) was pre-processed, refined, optimized, and minimized using the Protein Preparation Wizard module. The generated grid of enzyme was validated by extracting and re-docking of the co-crystallized ligand into the AChE. The pose of the re-docked ligand with the actual ligand was compared, and the RMSD value was calculated. The results of docking simulations were analyzed using glide XP visualizer, and the important active site interactions were analyzed along with the scoring functions.

4.7. Molecular dynamics simulations

The docked pose binding affinity and stability of compound **(22)** on the AChE (PDB Code: 1EVE) was evaluated using Desmond module of Schrödinger Maestro program. The explicit environment of water is created by soaking the ligand-protein complex in the TIP3P water molecules surrounded by orthorhombic water box. The neutralization of the prepared complex system was made by the addition of required counterions. The system was minimized using steepest descent minimization method with minimum 10 steps and cut-off using the short-range method as 9 Å. The maximum iterations for minimization were kept to 2000 and threshold of convergence was set to 1 kcal/mol/Å. The MD simulation run of 50 ns was performed by keeping the atoms (N), volume (V), and temperature (T) constant. Further, the system temperature was increased to 300 K, and the pressure was kept to 1.032 bar [52].

4.8. Statistical analysis

The values for each experimental group are expressed as Mean ± SEM. One-way ANOVA or two-way ANOVA was used to analyze differences between two groups (study and test) by statistical analysis software (Graph Pad Software, Inc., San Diego, CA).

Acknowledgments

The authors of the presented work would like to gratefully acknowledge the Indian Institute of Technology-Banaras Hindu University

(IIT-BHU), Varanasi for providing financial and necessary infrastructural facilities to carry out the experiments. The author would also like to thank the Department of Health Research, Ministry of Health and Family Welfares for approving Young Scientist Grant to Mr. Piyoosh Sharma in newer areas of Drugs Chemistry (V25011/215-HRD/2016-HR). We are also thankful to CSIR for providing financial support (CSIR-SRF File. No. 09/013(0697)/2017/EMR-1).

Appendix A. Supplementary material

^{1}H and ^{13}C NMR spectral characterization, QSAR, and *in vitro* enzyme kinetic study data can found in the supplementary section. Supplementary data to this article can be found online at https://doi.org/10.1016/j.bioorg.2018.10.009.

References

[1] Y. Hong-Qi, S. Zhi-Kun, C. Sheng-Di, Current advances in the treatment of Alzheimer's disease: focused on considerations targeting Aβ and tau, Transl. Neurodegener. 1 (1) (2012) 21.
[2] N. Öztaskın, P. Taslimi, A. Maraş, İ. Gülcin, S. Göksu, Novel antioxidant bromophenols with acetylcholinesterase, butyrylcholinesterase and carbonic anhydrase inhibitory actions, Bioorg. Chem. 74 (2017) 104–114.
[3] A. Akıncıoğlu, E. Kocaman, H. Akıncıoğlu, R.E. Salmas, S. Durdagi, İ. Gülçin, C.T. Supuran, S. Göksu, The synthesis of novel sulfamides derived from β-benzylphenethylamines as acetylcholinesterase, butyrylcholinesterase and carbonic anhydrase enzymes inhibitors, Bioorg. Chem. 74 (2017) 238–250.
[4] M. Wortmann, World Alzheimer report 2014: dementia and risk reduction, Alzheimers Dement. 11 (7) (2015) P837.
[5] A.S. Association, 2013 Alzheimer's disease facts and figures, Alzheimers Dement. 9 (2) (2013) 208–245.
[6] A.S. Association, 2014 Alzheimer's disease facts and figures, Alzheimers Dement. 10 (2) (2014) e47–e92.
[7] E.K. Perry, R. Perry, G. Blessed, B. Tomlinson, Changes in brain cholinesterases in senile dementia of Alzheimer type, Neuropathol. Appl. Neurobiol. 4 (4) (1978) 273–277.
[8] J.A. Hardy, G.A. Higgins, Alzheimer's disease: the amyloid cascade hypothesis, Science 256 (5054) (1992) 184.
[9] J.D. Grill, J.L. Cummings, Novel targets for Alzheimer's disease treatment, Expert Rev. Neurother. 10 (5) (2010) 711.
[10] Y. Stern, Cognitive reserve in ageing and Alzheimer's disease, Lancet Neurol. 11 (11) (2012) 1006–1012.
[11] W. Fischer, K.S. Chen, F.H. Gage, A. Björklund, Progressive decline in spatial learning and integrity of forebrain cholinergic neurons in rats during aging, Neurobiol. Aging 13 (1) (1992) 9–23.
[12] W. Fischer, F.H. Gage, A. Björklund, Degenerative changes in forebrain cholinergic nuclei correlate with cognitive impairments in aged rats, Eur. J. Neurosci. 1 (1) (1989) 34–45.
[13] D.G. Flood, P.D. Coleman, Neuron numbers and sizes in aging brain: comparisons of human, monkey, and rodent data, Neurobiol. Aging 9 (1988) 453–463.
[14] R. Morris, P. Garrud, J.A. Rawlins, J. O'Keefe, Place navigation impaired in rats with hippocampal lesions, Nature 297 (5868) (1982) 681–683.
[15] M.D. Lindner, A.H. Balch, C.P. Vandermaelen, Short forms of the “reference-” and “working-memory” Morris water maze for assessing age-related deficits, Behav. Neural Biol. 58 (2) (1992) 94–102.
[16] S.K. Sinha, S.K. Shrivastava, Synthesis, evaluation and molecular dynamics study of some new 4-aminopyridine semicarbazones as an antiamnesic and cognition enhancing agents, Bioorg. Med. Chem. 21 (17) (2013) 5451–5460.
[17] S.K. Sinha, S.K. Shrivastava, Design, synthesis and evaluation of some new 4-aminopyridine derivatives in learning and memory, Bioorg. Med. Chem. Lett. 23 (10) (2013) 2984–2989.
[18] S.K. Sinha, S.K. Shrivastava, Synthesis and evaluation of some new 4-aminopyridine derivatives as a potent antiamnesic and cognition enhancing drugs, Med. Chem. Res. 21 (12) (2012) 4395–4402.
[19] J. Trujillo-Ferrara, L.M. Cano, M. Espinoza-Fonseca, Synthesis, anticholinesterase activity and structure–activity relationships of m-Aminobenzoic acid derivatives, Bioorg. Med. Chem. Lett. 13 (10) (2003) 1825–1827.
[20] J. Correa-Basurto, I.V. Alcántara, L.M. Espinoza-Fonseca, J.G. Trujillo-Ferrara, p–Aminobenzoic acid derivatives as acetylcholinesterase inhibitors, Eur. J. Med. Chem. 40 (7) (2005) 732–735.
[21] N. Frimayanti, M.L. Yam, H.B. Lee, R. Othman, S.M. Zain, N.A. Rahman, Validation of quantitative structure-activity relationship (QSAR) model for photosensitizer activity prediction, Int. J. Mol. Sci. 12 (12) (2011) 8626–8644.
[22] H. Lineweaver, D. Burk, The determination of enzyme dissociation constants, J. Am. Chem. Soc. 56 (3) (1934) 658–666.
[23] A.D. Baddeley, G.J. Hitch, Development of working memory: should the Pascual-Leone and the Baddeley and Hitch models be merged? J. Exp. Child Psychol. 77 (2) (2000) 128–137.
[24] C. Germano, G.J. Kinsella, Working memory and learning in early Alzheimer's disease, Neuropsychol. Rev. 15 (1) (2005) 1–10.
[25] G.A. Radvansky, D.E. Copeland, Memory retrieval and interference: working memory issues, J. Mem. Lang. 55 (1) (2006) 33–46.
[26] N. Unsworth, G.J. Spillers, G.A. Brewer, Working memory capacity and retrieval limitations from long-term memory: An examination of differences in accessibility, Q. J. Exp. Psychol. 65 (12) (2012) 2397–2410.
[27] M.K. Healey, A. Miyake, The role of attention during retrieval in working-memory span: a dual-task study, Q. J. Exp. Psychol. 62 (4) (2009) 733–745.
[28] D.L. Nelson, L.B. Goodmon, Disrupting attention: the need for retrieval cues in working memory theories, Mem. Cognit. 31 (1) (2003) 65–76.
[29] P. Davies, A. Maloney, Selective loss of central cholinergic neurons in Alzheimer's disease, Lancet 308 (8000) (1976) 1403.
[30] B.J. Knowlton, M.S. Fanselow, The hippocampus, consolidation and on-line memory, Curr. Opin. Neurobiol. 8 (2) (1998) 293–296.
[31] S. Tronel, M.G. Feenstra, S.J. Sara, Noradrenergic action in prefrontal cortex in the late stage of memory consolidation, Learn. Mem. 11 (4) (2004) 453–458.
[32] C. Soriano-Mas, D. Redolar-Ripoll, L. Aldavert-Vera, I. Morgado-Bernal, P. Segura-Torres, Post-training intracranial self-stimulation facilitates a hippocampus-dependent task, Behav. Brain Res. 160 (1) (2005) 141–147.
[33] G. Kryger, I. Silman, J.L. Sussman, Structure of acetylcholinesterase complexed with E2020 (Aricept®): implications for the design of new anti-Alzheimer drugs, Structure 7 (3) (1999) 297–307.
[34] M. Kontoyianni, L.M. McClellan, G.S. Sokol, Evaluation of docking performance: comparative data on docking algorithms, J. Med. Chem. 47 (3) (2004) 558–565.
[35] S.K. Shrivastava, P. Srivastava, T. Upendra, P.N. Tripathi, S.K. Sinha, Design, synthesis and evaluation of some N-methylenebenzenamine derivatives as selective acetylcholinesterase (AChE) inhibitor and antioxidant to enhance learning and memory, Bioorg. Med. Chem. 25 (4) (2017) 1471–1480.
[36] S.K. Singh, S.K. Sinha, M.K. Shirsat, Design, synthesis and evaluation of some new 4-aminobenzoic acid derivatives as potential cognition enhancer, World J. Pharm. Pharm. Sci. 6 (8) (2017) 959–975.
[37] S. Kalva, D. Vinod, L.M. Saleena, Field-and Gaussian-based 3D-QSAR studies on barbiturate analogs as MMP-9 inhibitors, Med. Chem. Res. 22 (11) (2013) 5303–5313.
[38] T. Padrtova, P. Marvanova, K. Odehnalova, R. Kubinova, O. Parravicini, A. Garro, R.D. Enriz, O. Humpa, M. Oravec, P. Mokry, Synthesis, analysis, cholinesterase-inhibiting activity and molecular modelling studies of 3-(Dialkylamino)-2-hydroxypropyl 4-[(Alkoxy-carbonyl) amino] benzoates and their quaternary ammonium salts, Molecules 22 (12) (2017) 2048.
[39] A.V. Bogolubsky, Y.S. Moroz, P.K. Mykhailiuk, Y.V. Dmytriv, S.E. Pipko, L.N. Babichenko, A.I. Konovets, A. Tolmachev, Facile one-pot synthesis of 4-substituted semicarbazides, RSC Adv. 5 (2) (2015) 1063–1069.
[40] B. Yiğit, M. Yiğit, D. Barut Celepci, Y. Gök, A. Aktaş, M. Aygün, P. Taslimi, İ. Gülçin, Novel benzylic substituted imidazolinium, tetrahydropyrimidinium and tetrahydrodiazepinium salts: potent carbonic anhydrase and acetylcholinesterase inhibitors, ChemistrySelect 3 (27) (2018) 7976–7982.
[41] R.A.N. de Aquino, L.V. Modolo, R.B. Alves, Â. de Fátima, Synthesis, kinetic studies and molecular modeling of novel tacrine dimers as cholinesterase inhibitors, Org. Biomol. Chem. 11 (48) (2013) 8395–8409.
[42] P. Zdražilová, Š. Štěpánková, K. Komers, K. Ventura, A. Čegan, Half-inhibition concentrations of new cholinesterase inhibitors, Zeitschrift für Naturforschung C 59 (3–4) (2004) 293–296.
[43] A.G. Banerjee, N. Das, S.A. Shengule, P.A. Sharma, R.S. Srivastava, S.K. Shrivastava, Design, synthesis, evaluation and molecular modelling studies of some novel 5, 6-diphenyl-1, 2, 4-triazin-3 (2H)-ones bearing five-member heterocyclic moieties as potential COX-2 inhibitors: a hybrid pharmacophore approach, Bioorg. Chem. 69 (2016) 102–120.
[44] S.K. Shrivastava, B.K. Patel, P.N. Tripathi, P. Srivastava, P. Sharma, A. Tripathi, A. Seth, M.K. Tripathi, Synthesis, evaluation and docking studies of some 4-thiazolone derivatives as effective lipoxygenase inhibitors, Chem. Pap. 1–15 (2018).
[45] R. Morris, Developments of a water-maze procedure for studying spatial learning in the rat, J. Neurosci. Methods 11 (1) (1984) 47–60.
[46] R. Ojha, A.N. Sahu, A. Muruganandam, G.K. Singh, S. Krishnamurthy, Asparagus recemosus enhances memory and protects against amnesia in rodent models, Brain Cogn. 74 (1) (2010) 1–9.
[47] F.G. Davoodi, F. Motamedi, N. Naghdi, E. Akbari, Effect of reversible inactivation of the reuniens nucleus on spatial learning and memory in rats using Morris water maze task, Behav. Brain Res. 198 (1) (2009) 130–135.
[48] M. Jarvik, R. Kopp, An improved one-trial passive avoidance learning situation, Psychol. Rep. 21 (1) (1967) 221–224.
[49] I. Khromova, T. Voronina, V.A. Kraineva, N. Zolotov, P.T. Männistö, Effects of selective catechol-O-methyltransferase inhibitors on single-trial passive avoidance retention in male rats, Behav. Brain Res. 86 (1) (1997) 49–57.
[50] J.A. Lima, R.S. Costa, R.A. Epifânio, N.G. Castro, M.S. Rocha, A.C. Pinto, Geissospermum vellosii stembark: anticholinesterase activity and improvement of scopolamine-induced memory deficits, Pharmacol. Biochem. Behav. 92 (3) (2009) 508–513.
[51] O.H. Lowry, N.J. Rosebrough, A.L. Farr, R.J. Randall, Protein measurement with the Folin phenol reagent, J. Biol. Chem. 193 (1) (1951) 265–275.
[52] D. Shivakumar, J. Williams, Y. Wu, W. Damm, J. Shelley, W. Sherman, Prediction of absolute solvation free energies using molecular dynamics free energy perturbation and the OPLS force field, J. Chem. Theory Comput. 6 (5) (2010) 1509–1519.